Annealing twin development in austenite in steels after hot deformation

Garcia-Chao, Pablo; Nyyssönen, Tuomo; Ståhlkrantz, Adam; Magnusson, Hans

DOI
10.1016/j.matchar.2025.115012

Publication date
2025

Document Version
Final published version

Published in
Materials Characterization

Materials Characterization 224 (2025) 115012

Contents lists available at ScienceDirect

Materials Characterization

journal homepage: www.elsevier.com/locate/matchar

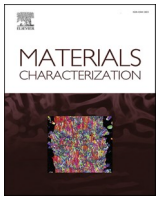

Annealing twin development in austenite in steels after hot deformation

Pablo Garcia-Chao [a,b,*], Tuomo Nyyssönen [a], Adam Ståhlkrantz [a], Hans Magnusson [a]

[a] Swerim AB, Isafjordsgatan 28A, 164 40 Kista, Sweden
[b] Department of Materials Science and Engineering, Delft University of Technology, Mekelweg 2, 2628 CD Delft, the Netherlands

ARTICLE INFO

Keywords:
Annealing twinning
Recrystallization
Grain growth
Steel
Electron backscatter diffraction
Boundary tortuosity
Dislocation density

ABSTRACT

Twinning development in the annealing of hot-deformed austenite in steels has often been suggested to play a relevant role in e.g. the evolution of grain size and texture across the process. Nevertheless, the phenomenon has not been systematically studied. In this view, a detailed assessment of annealing twin boundary evolution in austenite after hot deformation is carried out for the first time. Particularly, three materials are examined via electron backscatter diffraction (EBSD): a stainless steel, a carbon steel, and a Ni-30Fe alloy. Results demonstrate that twin boundaries form via recrystallization, and disappear by grain growth. However, unlike previously reported for lower annealing temperature in nickel, the number of twins per recrystallized grain does not increase throughout recrystallization. On the contrary, it stagnates before its end, upon activation of concomitant grain growth. Additionally, twin density increases with lower deformation/annealing temperature, higher strain rate, and higher applied strain. This has been rationalized via the higher resultant stored energy, which increases the density of microstructural discontinuities inside the deformed matrix (and, thereby, the rate of growth accidents). By contrast, no correlation has been observed between the measured boundary tortuosity and twin density. While Σ3 and Σ9 boundaries appear at the same rate during recrystallization, Σ9 ones disappear considerably more quickly with grain growth. Finally, the twin density trends examined after EBSD parent austenite reconstruction on the carbon steel have all been consistent. Consequently, that method represents a promising approach to analyze annealing twinning in steels that undergo phase transformations upon cooling.

1. Introduction

When annealed at elevated temperature, deformed metals undergo recrystallization and subsequent grain growth. Besides, twin boundaries form during annealing in all face-centered cubic (FCC) metals, except for aluminum [1]. The most commonly observed annealing twin boundaries exhibit the orientation relationship of the $\sum 3$ coincident site lattice (CSL) boundaries [2]. Although their formation is poorly understood, the so-called 'growth accident' theory has been proposed [3–7]. By this theory, twin boundaries appear as a grain boundary migrates, whenever a change takes place in the stacking sequence of close-packed planes: e.g., the bars in the sequence ABCA|CBACBACB|CABC… [2,5]. Annealing twin boundaries can also exhibit the orientation relationships of $\sum 3^m$ boundaries, m being 2, 3… For example, $\sum 9$ boundaries form when two $\sum 3$ boundaries impinge during annealing [8]. In turn, when a $\sum 3$ and a $\sum 9$ boundary meet, either a $\sum 27$ or another $\sum 3$ boundary can result. In practice, the vast majority of annealing twin boundaries found in FCC metals are $\sum 3$ or $\sum 9$ [8–10].

Despite far-reaching effects on e.g. mechanical behavior [11–16], annealing twins in FCC metals have started attracting more attention only recently. A review of these recent efforts has been conducted by Bozzolo and Bernacki [12]. Among these studies, Jin et al. thoroughly quantified twin density evolution during recrystallization and subsequent grain growth for one case: pure nickel deformed at room temperature, and then annealed at low temperature [1,7,17]. The effect of deformation/annealing conditions was also analyzed, namely the applied strain, initial grain size, and annealing temperature [7]. Nevertheless, a limitation in this work was the lack of distinction between Σ3 and Σ9 twin boundaries [1,7,17]. Moreover, a similar study is missing for another industrially relevant annealing process: that of austenite in steels. In the industrial processing of steels, recrystallization and grain growth occur in the austenite phase upon hot rolling, after the

Abbreviations: BCC, Body-centered cubic; CSL, Coincidence site lattice; EBSD, Electron backscatter diffraction; FCC, Face-centered cubic; FEG-SEM, Field emission gun scanning electron microscope; FTB, Former twin boundary; GND, Geometrically necessary dislocation; GOS, Grain orientation spread; IPF, Inverse pole figure; HAB, High-angle boundary; LAB, Low-angle boundary; ND, Normal direction; SFE, Stacking fault energy.

* Corresponding author at: Department of Materials Science and Engineering, Delft University of Technology, Mekelweg 2, 2628 CD Delft, the Netherlands.
E-mail address: p.garciachao@tudelft.nl (P. Garcia-Chao).

https://doi.org/10.1016/j.matchar.2025.115012
Received 29 January 2025; Received in revised form 31 March 2025; Accepted 3 April 2025
Available online 4 April 2025

material is deformed by each successive rolling pass. Due to the practical importance of the process, the annealing response of austenite under these conditions has attracted considerable research over the years. The main interest has been to predict the resultant grain size and texture, together with the kinetics of recrystallization [18–22]. These parameters control the anisotropy, mechanical properties and processing response of the material during subsequent processing steps, as well as in the final state.

In this sense, specific reasons exist why the quantification and understanding of the concomitant twinning are needed to predict, with sufficient accuracy, grain size and texture evolution in the annealing of austenite in steels. This is the case for both recrystallization and grain growth. For instance, Haase et al. and Shankar et al. could not reproduce the evolution of texture during recrystallization without including the new orientations created by the annealing twinning [19,22]. About the nucleation of recrystallization, Garcia-Chao et al. found that roughly one fourth of the recrystallized grains nucleate at the junctions between twin boundaries and general high-angle boundaries (HABs) [23]. Quantitatively reproducing the density of nucleation is a requirement to predict the grain size after recrystallization [2,18]. Similarly, Bhattacharyya et al. observed that the junctions between twin boundaries and general HABs considerably retard grain growth (thus, strongly affecting the resultant grain size) [24,25]. Such junctions are relatively immobile [24,25], owing to the low mobility intrinsic to Σ3 boundaries in FCC metals [26,27].

Additionally, the annealing of austenite in steels differs from the case considered by Jin et al. [1,7,17] in two main ways, both expected to affect annealing twin evolution:

i. The material has significantly lower stacking fault energy (SFE). SFE is understood to determine the probability of annealing twin formation in FCC metals, with twin densities consistently observed to increase with lower SFE [6,8,11,24]. For the case of interest here, Charnock and Nutting measured an SFE of 120 ± 8 mJ/m^2 for pure nickel, against 75 ± 12 mJ/m^2 for pure iron (with the latter value not significantly affected by carbon additions up to 0.8 wt%) [28]. For stainless steels, SFE is even lower: e.g., 25–35 mJ/m^2 for 304 L and 316 L [29–31]. Hence, increased annealing twinning would be expected for austenite in steels compared to pure nickel.
ii. Deformation and annealing occur at high temperature (> 850 °C). By contrast, only deformation at room temperature, with subsequent annealing at 350–450 °C, was considered by Jin et al. [1,7,17]. Firstly, the high deformation temperature renders some deformation parameters relevant, which do not play a role in room-temperature deformation. For instance, strain rate is well-known to strongly affect microstructural evolution in annealing after hot deformation [2]. Likewise, hot deformation operations (e.g., hot rolling) are performed at a range of temperatures, while only one annealing temperature was studied in [1,7,17]. Despite this, the effects of deformation temperature and strain rate on annealing twin formation have not been studied [7]. Additionally, during thermomechanical processing at high temperature, both deformation and annealing occur at the same high temperature, either simultaneously or consecutively. The effects of deformation and annealing temperature become thus intertwined, which is not the case at lower temperature. Finally, no parameter is widely accepted to date to explain the different twin densities resulting from diverse thermomechanical processing conditions. On the one hand, classical research has often related higher twin densities to quicker boundary migration rates [1,6,32,33]. The underlying assumption has been that growth accidents are more likely for more rapid boundary motion [5]. However, this hypothesis has failed to explain the insensitivity of twin density to annealing temperature observed by Jin et al., for the same deformed microstructure [7]. The same authors have explained the effect of deformation and annealing parameters on twin density for their case via the tortuosity of the boundary migration front during recrystallization [7]. Growth accidents (and, hence, annealing twin formation) can only occur when one of the {111} octahedral planes is parallel to the migrating boundary [3,5]. For a given crystallographic orientation, the number of sites where this condition is fulfilled should naturally increase for a more tortuous boundary [7]. Nevertheless, Jin et al. checked the relationship between twin density and boundary tortuosity for three deformation conditions in pure nickel only [7]. The relationship is yet to be tested for other materials and conditions, as the own authors recommended [7].

Finally, characterization of annealing twin formation is simple for materials in which the FCC austenite phase is stable or metastable at room temperature. However, it is prohibitively difficult in carbon steels, where the FCC austenite transforms into other phases when cooled to room temperature. This means that the microstructure of austenite (including the twin boundaries) cannot be accessed via regular characterization techniques, like electron backscatter diffraction (EBSD). To address this issue, EBSD-based methods have been developed, able to reconstruct parent austenite microstructures from their martensite phase product. Such methods have been shown to correctly represent both the texture evolution and kinetics of recrystallization [34]. Furthermore, they have often been claimed to be able to reconstruct annealing twin boundaries [34–39]. However, whether such reconstruction methods produce consistent twin density trends, and can thus be used to analyze annealing twinning in carbon steels, has not been proved.

Within this context, the goal of this study is to elucidate the evolution of annealing twinning in austenite in steels after hot deformation, including recrystallization and subsequent grain growth. This evolution is evaluated via EBSD after deformation in different conditions, selected among those relevant in the industrial hot rolling of the specific grade. Additionally, emphasis is placed on understanding the effects of the temperature of deformation/annealing, strain rate and applied strain. Those effects are then rationalized through factors that can potentially explain twin density differences among deformation conditions (including recrystallization front tortuosity). Finally, attention is paid to the distinct evolutions of Σ3 and Σ9 boundaries. As materials, a stainless steel (316 L) and a low-alloy carbon steel have been chosen. For 316 L, the austenite present at high temperature can be characterized with regular EBSD. For the carbon steel, on the other hand, the parent austenite must be reconstructed from the orientation map measured on martensite. Hence, the carbon steel is used to explore the suitability of parent austenite reconstruction methods to examine annealing twinning. Finally, experiments are also conducted on a Ni-30Fe alloy. This alloy has essentially the same SFE as carbon steels (~74 mJ/m^2 [28]), which should impart analogous twinning behavior. By contrast, Ni-30Fe stays in the austenite phase when cooled to room temperature. This makes it possible to characterize the microstructure present at high temperature via regular EBSD, including the annealing twins.

2. Experimental methods

2.1. Materials

Typical commercial grades corresponding to a stainless steel (316 L) and a low-alloyed carbon steel (Fe-C-Mn steel) were selected for this study, together with a Ni-30Fe alloy. Ni-30Fe has similar SFE to the austenite in carbon steels [28]. However, it stays in austenite phase when quenched to room temperature. Hence, unlike for carbon steels, the high-temperature microstructure can be readily characterized through room-temperature techniques. At the same time, the dislocation behavior of FCC crystals is defined by their SFE. As a result, Ni-30Fe has been extensively used as a model [40] for the plastic deformation and recrystallization behavior of austenite in steels at high temperature [23,26,41–46]. Similarly, the relationship between annealing twin formation and SFE (Section 1) suggests that this alloy should also constitute

a good model for carbon steels in terms of twinning. The Ni-30Fe alloy used here was supplied by Goodfellow Ltd. UK, in its regular commercial condition. The chemical compositions of the three alloys are displayed in Table 1.

2.2. Thermo-mechanical processing

Two types of experiments were performed. Firstly, recrystallization experiments were carried out to characterize twin development during recrystallization, and the effect of deformation/annealing parameters. For the carbon steel, and one of the deformation conditions of Ni-30Fe (900 °C, see Table 2), significantly longer annealing times than needed to complete recrystallization were applied, to also extract information on grain growth. Secondly, soaking experiments were carried out on 316 L, to obtain extra data on twin evolution upon grain growth.

In the recrystallization experiments, specimens corresponding to the commercial state of each material were deformed at high temperature. This deformation temperature was then held for a certain annealing time, before quenching to room temperature. Afterwards, the as-quenched samples were subjected to EBSD characterization. For each deformation condition, various annealing times were applied to different specimens, to obtain information at different stages of recrystallization. The deformation conditions and annealing times employed for each material are shown in Table 2. The initial state before deformation was always fully recrystallized. The average grain size measured immediately before deformation was of approximately 20 μm for 316 L, 50 μm for the carbon steel, and 90 μm for Ni-30Fe. In the soaking experiments, 316 L specimens were held at different temperatures (900, 1100 and 1150 °C) for a time of 300 s, directly from the commercial material condition. By these means, different degrees of grain growth were imparted, without (unlike in the recrystallization experiments) any previous deformation. Subsequently, the soaked samples were quenched, and subjected to EBSD analysis. To avoid any confusion, the 316 L samples subjected to the recrystallization and soaking experiments are referred to below as 316 L-1 and 316–2, respectively.

The experiments corresponding to 316 L (both 316 L-1 and 316–2) and the carbon steel were carried out at Swerim AB, in a Gleeble 3800 simulator with a Hydrawedge module. Standard cylindrical Gleeble specimens were prepared, having 15 mm in length and 10 mm in diameter. Samples were water-quenched in the Gleeble after the treatments. The experiments on Ni-30Fe were performed at Delft University of Technology, in a Bähr DIL 805 A/D dilatometer. Standard cylindrical specimens with a length of 10 mm and a diameter of 5 mm were employed. Quenching with helium was carried out inside the dilatometer. More information on the Ni-30Fe experiments is given in [23]. Deformation consisted of uniaxial compression in all cases.

For each deformation condition studied in the recrystallization experiments, one specimen was quenched immediately after deformation. For those specimens, an annealing time of ~0.5 s was measured (Table 2). This was the shortest time possible between the end of deformation and the start of cooling with both the Gleeble and the dilatometer.

2.3. Microstructural characterization via EBSD

All the specimens were characterized in a cross-section perpendicular to the cylindrical axis, as close as possible to mid-sample length, and at the center of the cross-section. The samples were mechanically ground and polished using conventional metallographic methods. The last polishing step was conducted with commercial colloidal silica suspensions. For the stainless and carbon steels, the EBSD analysis was carried out at Swerim AB, in a field emission gun scanning electron microscope (FEG-SEM) Zeiss Gemini 450. The FEG-SEM was operated at 15 kV, with beam current of 15 nA and working distance of approximately 15 mm. The EBSD patterns were captured with an Oxford Instruments Symmetry detector, employing Aztec version 6.1 as the acquisition software. The Ni-30Fe samples deformed at 1000 °C with applied strain of 0.2 and strain rate of 1 s^{-1} were scanned at Delft University of Technology, in a Thermo Fisher Helios G4 PFIB UXe FEG-SEM. This FEG-SEM was equipped with an Ametek EDAX Hikari Plus EBSD detector, and APEX 2.5.1 as the acquisition software. The acquisition parameters were an accelerating voltage of 20 kV, beam current of 6.4 nA, and working distance of approximately 6 mm. The EBSD acquisition for the rest of Ni-30Fe samples was performed at Tata Steel Nederland, and is described in [23]. For 316 L, minimum areas of 0.1 and 1.0 mm^2 were scanned in the recrystallization (316 L-1) and soaking (316 L-2) experiments, respectively. The step size was 0.2 μm for the recrystallization specimens, and 0.5 μm for the soaking ones. For the carbon steel, the minimum area scanned was 0.1 mm^2, using a step size of 0.2 μm. For Ni-30Fe, a minimum area of 1.5 mm^2 was scanned, with a step size of 0.5 μm. The resultant maps were fully austenitic for Ni-30Fe, mostly martensitic for the carbon steel, and mostly austenitic for 316 L. For the two latter materials, lower fractions than 0.1 and 0.6 % of austenite and body-center cubic (BCC) phase, respectively, were indexed.

For the carbon steel, parent austenite orientation maps were reconstructed from the EBSD data. The reconstruction was conducted on Matlab R2023b running with MTEX 5.11.1. Firstly, retained austenite and pixels fully surrounded by a misorientation of 15° were removed. A grain map was then constructed with a misorientation of 2°, from which a representative austenite-to-martensite orientation relationship was derived using the standard iterative method in MTEX [35] ('quantile' set to 0.6). For each grain in this map, parent orientation solutions were obtained via five iterations of the MTEX variant graph algorithm [36] (threshold of 4°, tolerance of 2° and inflation power set to 1.05). The grain map was then merged for a threshold of 5°, with an additional merging of 15° applied to grains smaller than 2 μm. Individual solutions were then attempted to be found for any remaining child grains. In each map, over 99 % of the child grains were reconstructed into parent austenite with this method. Finally, individual parent orientation solutions were calculated for each orientation pixel in the original martensite map.

For 316 L and Ni-30Fe, the EBSD data were directly postprocessed in AztecCrystal 6.1 and OIM Analysis 8, respectively. For the carbon steel, the reconstructed EBSD data were postprocessed further in MTEX 5.11.1. A Kuwahara filter [47] was applied in all cases to minimize the noise in the maps. For 316 L, pixels indexed as BCC were excluded from the calculations. Deformed and recrystallized grains were then separated in terms of their mean grain orientation spread (GOS). Grains

Table 1
Chemical compositions of the studied alloys. Contents are given in weight percent.

Alloy	Fe	Ni	C	Si	Mn	Cr	Mo	Cu	Nb
316 L	Bal.	10	0.02	0.5	1.9	17	2	0.5	–
Ni-30Fe	31	Bal.	0.01	–	0.01	–	–	–	–
Carbon steel	Bal.	–	0.15	–	1.4	–	–	–	0.01

Table 2
Deformation conditions and annealing times examined in the recrystallization experiments performed for the different alloys in the study.

Alloy	Temperature (°C)	Strain	Strain rate (s^{-1})	Annealing times (s)
316 L-1	1000	0.4	1	0.5, 6.5, 12, 24, 36
	900	0.2	1	1, 2, 5, 10, 20, 50, 100, 200, 500, 1000
Ni-30Fe	1000	0.2	1	0.5, 1, 2, 5, 10, 20
	1000	0.2	10	0.5
	1000	0.4	10	0.5, 1
Carbon steel	950	0.2	10	0.5, 20, 500
	950	0.4	10	0.5, 20, 500

smaller than 4 and 15 pixels were excluded from the maps with step sizes of 0.5 and 0.2 μm, respectively. Grains were constructed with minimum misorientations of 15° and 5° in maps having recrystallized area fractions lower and higher than 10 %, respectively. CSL boundaries were detected according to their orientation relationships: 60°⟨111⟩ for ∑3 boundaries, and 38.9°⟨110⟩ for ∑9 boundaries [26]. In this detection, angular tolerances were allowed following Brandon's criterion [48]. Grain sizes are given as equivalent circle diameters. The densities of geometrically necessary dislocations (GNDs) were calculated with the method in [49], based on 1st-order neighbors. For this purpose, ⟨110⟩ slip systems and a Burgers vector length of 0.2518 nm were considered [50].

Unless otherwise stated, black and gray lines in the presented EBSD maps indicate boundaries with higher misorientation than 15° (i.e., HABs), or misorientations between 5 and 15° (i.e., low-angle boundaries, or LABs). White lines are boundaries identified as CSL (of either the Σ3 or the Σ9 type). The vertical direction of the EBSD maps is always the compression direction.

Annealing twinning in the recrystallized grains of the analyzed maps was evaluated through the number of twin boundaries per recrystallized grain n, and twin boundary density p [7]:

$$n = d_{RX}/c_{RX} - 1 \tag{1}$$

$$p = L_{tb}/S_{RX} \times 2/\pi \tag{2}$$

where d_{RX} and c_{RX} are the average recrystallized grain sizes excluding and including twin boundaries from the grain construction; L_{tb} is the length of the twin boundaries detected in the recrystallized grains of the EBSD map; and S_{RX} is the area of those recrystallized grains. S_{RX} was considered more appropriate than the total EBSD map area, which had been used in [7].

The number of twin boundaries inside individual recrystallized grains was derived with the specific tool in AztecCrystal 6.1. The Pearson correlation coefficients and the linear regression plots were obtained using the Pandas and Seaborn libraries of Python, respectively.

The average tortuosity of the recrystallization front τ was calculated as [7]:

$$\tau = L_{RF}/R_{RF} \tag{3}$$

where L_{RF} and R_{RF} represent the combined geodesic (actual) and Euclidean (end-to-end as a straight line) lengths of all the boundaries between recrystallized and deformed grains in the corresponding EBSD maps. L_{RF} and R_{RF} were obtained from [7]:

$$L_{RF} = L_t - L_{RX} - L_{def} \tag{4}$$

$$R_{RF} = R_t - R_{RX} - R_{def} \tag{5}$$

where L_t and R_t, L_{RX} and R_{RX}, and L_{def} and R_{def} are the combined geodesic/Euclidean lengths of all the boundaries, all the boundaries between recrystallized grains and all the boundaries between deformed grains in the EBSD maps. The combined geodesic and Euclidean distances in such three different partitions were derived with OIM Analysis 7.3. For this purpose, the maximum deviation allowed between the reconstructed end-to-end straight boundary and the actual boundary was 30 times the map step size (the largest allowed by the software). If this value is exceeded, the software reconstructs the boundary as a zigzag line instead of as a simple straight one. Yet, simple straight boundaries were obtained for nearly all the examined boundaries.

3. Results

In Section 3, the evolution of twinning during annealing is first analyzed sequentially for the materials for which the EBSD analysis could be directly performed in the austenite phase (316 L and Ni-30Fe). Twin development upon recrystallization is examined in Section 3.1, with the microstructures obtained at the end of recrystallization presented in Section 3.2. Twin evolution during grain growth after the completion of recrystallization is then described in Section 3.3. Afterwards, twin evolution as studied via EBSD parent austenite reconstruction for the carbon steel is shown in Section 3.4, considering the particularities of the application of this method.

3.1. Twin development during recrystallization

In this section, the evolution of annealing twinning upon recrystallization is examined for 316 L-1, and Ni-30Fe deformed and annealed at two different temperatures (900 and 1000 °C), with equal strain rate and applied strain (1 s^{-1} and 0.2). The average values for the entire microstructures are summarized in Fig. 1 (316 L-1), Fig. 2 (Ni-30Fe at 900 °C) and Fig. 3 (Ni-30Fe at 1000 °C). The plots depict the evolution upon recrystallization of the number of twin boundaries per recrystallized grain n, and the main microstructural variables describing recrystallization: recrystallized fraction (f_{RX}), and average size of the recrystallized grains (d_{RX}). Microstructures within each recrystallization process are given in Fig. 4 (316 L-1), Fig. 5(a)-(b) (Ni-30Fe at 900 °C) and Fig. 5(c)-(e) (Ni-30Fe at 1000 °C).

In the three recrystallization processes, recrystallized fraction and grain size followed the usual [1,21,26] sigmoidal trend with annealing time (Fig. 1(a), Fig. 2(a) and Fig. 3(a)). At the same time, also in the three processes, n increased steadily from a value close to zero at the start of recrystallization (Fig. 1(b), Fig. 2(b) and Fig. 3(b)). This implies that annealing twin boundaries are created during recrystallization, as suggested by Jin et al. for pure nickel deformed at room temperature, then annealed at low temperature [1,7]. However, in this case, n stagnated well before the end of recrystallization. For 316 L-1, the stagnation was only observed after a recrystallized fraction of ~80 % (Fig. 1(b)). For Ni-30Fe, n ceased to increase as early as for recrystallized fractions of ~40 % (Fig. 2(b) and Fig. 3(b)). The behavior of the present materials contrasts with the findings in [1,7], where n increased linearly with d_{RX} throughout recrystallization. The increase continued beyond recrystallized fractions of 95 % [1,7], irrespective of the applied strain and annealing temperature [7].

Additionally, Fig. 6 displays the number of annealing twin boundaries inside each recrystallized grain as a function of the size of the grain. Data correspond to the grains captured for 316 L-1 after annealing for 0.5 (Fig. 6(a)) and 6.5 s (Fig. 6(b)). For both times, the plots show a clear positive linear correlation between number of twins and grain size: larger grains tended to contain more twin boundaries. This correlation is illustrated by the Pearson coefficient: 0.64 after 0.5 s, and 0.79 after 6.5 s (with values higher than 0.5 typically regarded as strong correlation [51]). The correlation is enhanced by longer annealing due to the greater growth undergone by the recrystallized grains, which leads to a larger range of grain sizes present. These results indicate that twin boundaries appear during recrystallization via the growth of the recrystallizing grains: larger distance of growth (i.e., larger grain size) unavoidably led to more twin boundaries formed in the recrystallized grain.

3.2. Annealing twin density at the end of recrystallization

The annealing twin statistics (i.e., n and p) at the end of recrystallization are provided in Table 3 for the materials and deformation conditions examined. p is the density of twin boundaries per analyzed area, i.e. it gives the total amount of twinning in the recrystallized microstructure. Hence, p is the appropriate variable to compare the tendency for twinning among different recrystallization processes. By contrast, n is the number of twin boundaries per recrystallized grain, and is thus a function of both that tendency, and the distance covered by each grain upon its growth into the deformed grains (since twin boundaries are formed during that growth, as shown in the previous section). In turn,

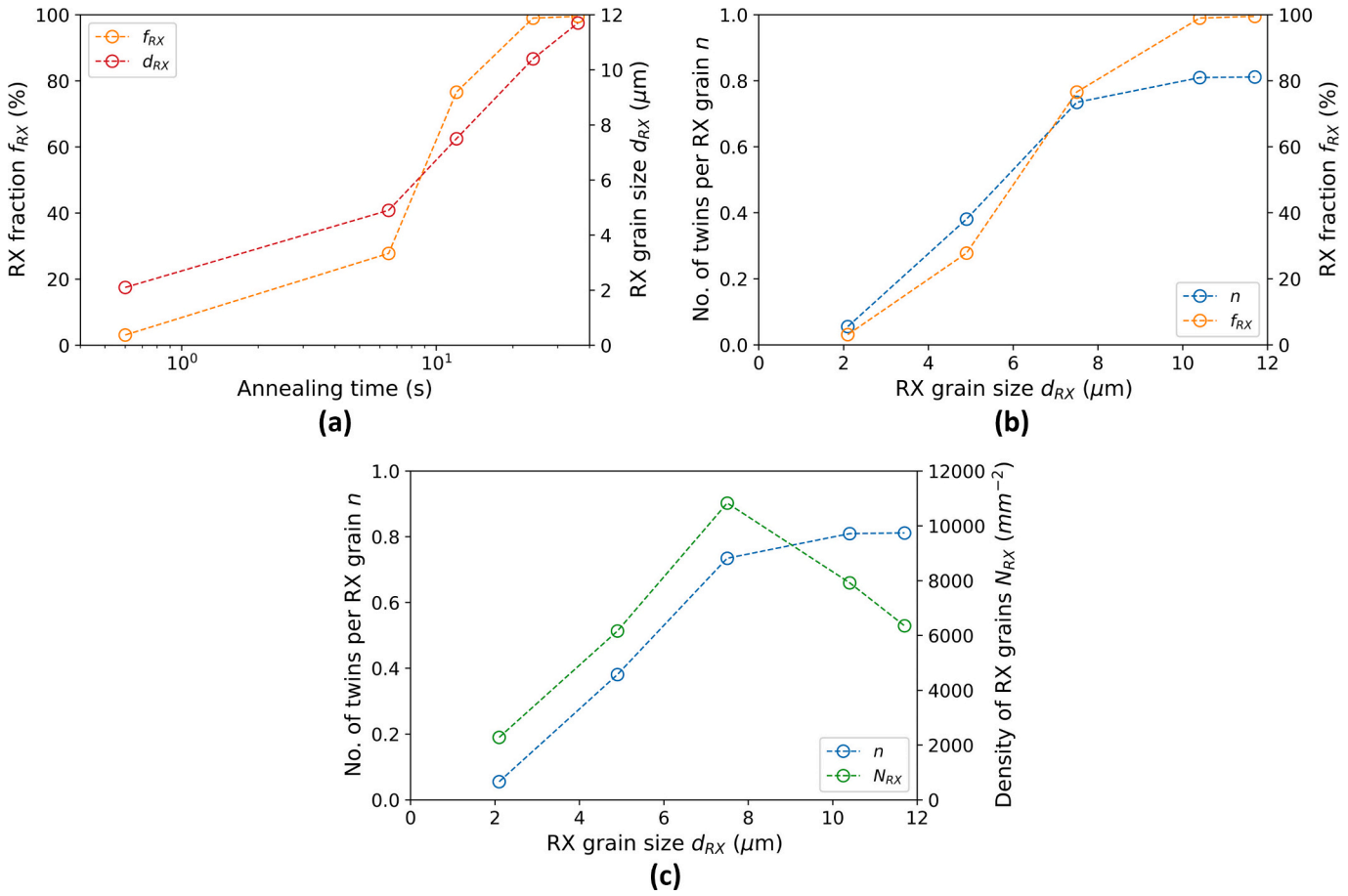

Fig. 1. Results corresponding to the recrystallization experiments performed for 316 L-1: (a) evolution of recrystallized (RX) fraction f_{RX} and grain size d_{RX} with annealing time; (b, c) number of twin boundaries per recrystallized grain n as a function of recrystallized grain size d_{RX}, plotted together with (b) recrystallized fraction f_{RX}, and (c) the density of recrystallized grains N_{RX}.

that distance depends on the density of the recrystallized grains formed, which will differ among recrystallization processes: more recrystallized grains mean smaller growth distance into the deformed structure available for each, due to the earlier impingement. This will reduce the number of twins formed per recrystallized grain (even when the tendency for twinning for that material and deformation condition does not change).

Firstly, the results for Ni-30Fe deformed at 900 and 1000 °C with equal applied strain and strain rate indicate that p increased with lower deformation temperature (increase of ~20 %, see Table 3). Fig. 7 demonstrates that this was the case not only at the end of recrystallization, but also throughout the process, irrespective of the recrystallized fraction. Although the temperature of annealing was also different for these two cases in Table 3, Jin et al. proved that neither p nor n is affected by annealing temperature [7]. This was done by annealing the same deformation condition at different temperatures [7]. In the present case, performing deformation and annealing at different temperatures is not possible. The reason is that, in the hot deformation of austenite, recrystallization times are close to the heating or cooling times required for temperature shifts after deformation. Accordingly, previous research on the effect of temperature on recrystallization in austenite has not included temperature changes between deformation and annealing [18,21,52,53]. Consequently, these results suggest an increase in the probability of twinning during recrystallization when deformation temperature is lowered. Regarding the other parameters in Table 3, n remained largely unchanged between 900 and 1000 °C. At the same time, the recrystallized grain size d_{RX} was smaller for 900 °C (i.e., the density of recrystallized grains N_{RX} was higher, see Fig. 3(c) and Fig. 2(c)). This implies that the stronger overall probability of twinning for the lower temperature was compensated for, in terms of n, by a smaller growth distance covered by each grain. Larger recrystallized grain sizes for higher temperature of deformation have usually been observed in the annealing of austenite [2,52,53]. The present results indicate the specific reason for this behavior: more grain growth occurring at the higher temperature. This is despite the higher nucleation density also measured for that temperature (which, in contrast with the actual observation, would have reduced the recrystallized grain size): ~890 grains/mm^2 after 2 s at 1000 °C (Fig. 2(c)), against ~760 grains/mm^2 after 20 s at 900 °C (Fig. 3(c)). The greater degree of grain growth is indicated by the stronger subsequent reduction in recrystallized grain density up to the end of recrystallization: the final value was ~500 grains/mm^2 at 1000 °C (20 s in Fig. 3(c)), but ~620 mm^{-2} at 900 °C (100 s in Fig. 2(c)). Finally, the lower temperature at 900 °C delayed recrystallization kinetics. This is also the general observation for recrystallization in austenite [18,21,52,53]. The reason is the lower annealing temperature after deformation, which retards the migration of the recrystallizing boundaries [2].

Similarly, the effect of strain rate on annealing twin statistics is illustrated in Table 4. As defined by Eq. (2), p is a function of the recrystallized volume. Hence, for p to be comparable among deformation conditions, recrystallized fraction f_{RX} must be the same. Considering this, Table 4 shows the twinning statistics for Ni-30Fe recrystallized up to an f_{RX} of ~10 %, after deformation with different strain rates (1 to 10 s^{-1}), and equal temperature and applied strain (1000 °C and 0.2). In particular, the table indicates that increasing strain rate from 1 to 10 s^{-1} strongly affected twin density: p nearly doubled. This time, the number

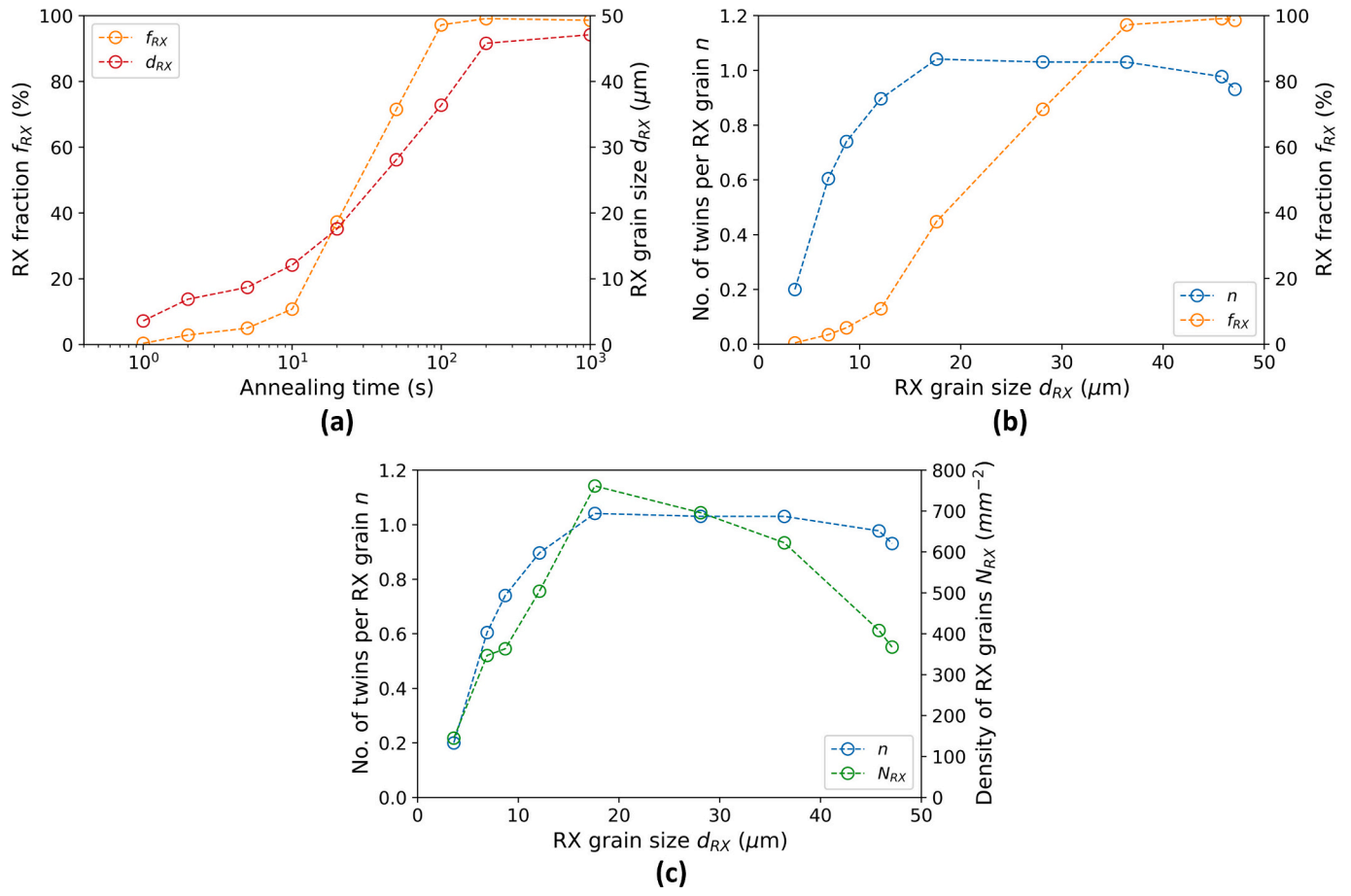

Fig. 2. Results corresponding to Ni-30Fe deformed and annealed at 900 °C: (a) evolution of recrystallized (RX) fraction f_{RX} and grain size d_{RX} with annealing time; (b, c) number of twin boundaries per recrystallized grain n as a function of recrystallized grain size d_{RX}, plotted together with (b) recrystallized fraction f_{RX}, and (c) the density of recrystallized grains N_{RX}.

of twin boundaries per recrystallized grain n increased accordingly, by about two thirds. This is because the increase of strain rate did not significantly alter the average size of the recrystallized grains (Table 4) or their density (Fig. 3(c)). As a result, recrystallized grains roughly covered the same distance of growth into the deformed structure. Interestingly, the effect of increasing strain rate from 1 to 10 s^{-1} on n was quantitatively similar to that of reducing deformation temperature from 1000 to 900 °C: from ~0.5 to ~0.85–0.90, for a similar d_{RX} of 10–12 μm (Table 4). In addition, increasing strain rate reduced the time required to reach an f_{RX} of ~10 %. Acceleration of recrystallization kinetics with higher strain rate is usually observed for recrystallization in austenite [21,53]. This agrees with the higher stored energy expected after deformation, which enhances both the nucleation and growth of recrystallized grains [2,54,55].

Apart from this, Table 3 shows that deforming Ni-30Fe at 1000 °C to a strain of 0.4 and with a strain rate of 10 s^{-1} led to considerably higher p than when employing the same temperature, but a lower applied strain and strain rate (0.2 and 1 s^{-1}). The higher p was present throughout recrystallization, at least in the portion of the process that could be captured by EBSD (Fig. 7). In this regard, owing to the rapid kinetics inherent to those deformation parameters, recrystallized fractions lower than 50 % could not be captured for the higher strain and strain rate. That would have implied shorter annealing than the minimum time possible between end of deformation and start of quenching (~0.5 s with either dilatometer or Gleeble, which was also the time for 50 % recrystallization with those deformation conditions, see Fig. 3(a)). Quicker kinetics for higher strain and strain rate are typically observed in recrystallization in austenite [21,52,53,56]. Regarding the higher p under those conditions, it can be related to the higher strain rate, as explained in the previous paragraph. Nevertheless, the higher applied strain should also have contributed. In this sense, both Jin et al. and Li et al. found a monotonic increase in twin density after recrystallization, for higher cold-rolling reduction imparted to pure nickel [7,33]. Furthermore, higher twin densities after recrystallization were measured in alpha-brass near a hardness indentation compared to far from it [3], and in copper after surface grinding [5], than in a non-ground sample. Both the indentations and grinding were applied before recrystallization, and increase the plastic deformation in the microstructure [3,5]. In the present case, this higher probability of twinning with higher applied strain and strain rate did not give rise to an increase of n. On the contrary, n did not significantly change (Table 3). The reason is that, again, the higher probability of twinning was counteracted by higher density of recrystallized grains (see the smaller d_{RX} in Table 3). Smaller recrystallized grain size for higher strain and strain rate is the usual observation in recrystallization of austenite [21,52,53,56]. Noteworthily, the value of p shown by Ni-30Fe after recrystallization with strain of 0.4 and strain rate of 10 s^{-1} was nearly identical to that of 316 L-1 (Table 3). This was despite the lower strain rate utilized for 316 L-1.

3.3. Twin development during grain growth

In this section, annealing twin evolution is evaluated during grain growth, after the end of recrystallization. For this purpose, Table 5 includes data corresponding to three sets of experiments. The microstructures at the beginning of each experiment set were fully or almost

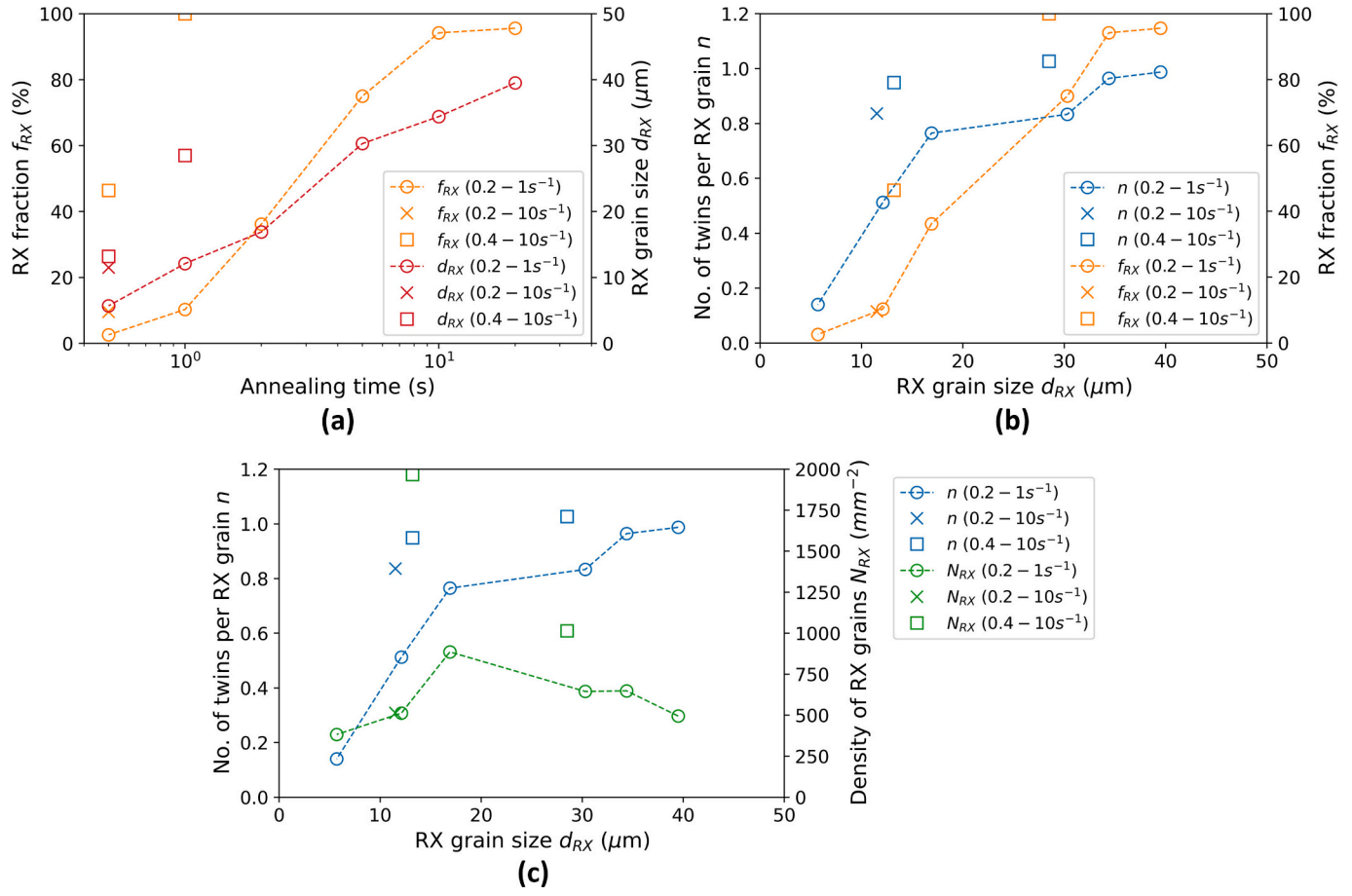

Fig. 3. Results corresponding to Ni-30Fe deformed and annealed at 1000 °C, with different strains and strain rates: (a) evolution of recrystallized (RX) fraction f_{RX} and grain size d_{RX} with annealing time; (b, c) number of twin boundaries per recrystallized grain n as a function of recrystallized grain size d_{RX}, plotted together with (b) recrystallized fraction f_{RX}, and (c) the density of recrystallized grains N_{RX}.

fully recrystallized (minimum f_{RX} = 97 %). This means that the final microstructures in each set differed only in the degree of grain growth sustained. Particularly, two sets of experiments were conducted on 316 L. In the first one (316–1), samples that underwent the hot deformation in Section 3.1 were subjected to longer holding times after deformation than required for full recrystallization (and at the same temperature of deformation/recrystallization). Hence, the initial condition for grain growth in 316–1 was the fully recrystallized state in Section 3.1 (see Fig. 1(d)). In the second set (316–2), 316 L samples were annealed at different temperatures for the same holding time, directly from the as-received, commercial state. Therefore, the initial condition for grain growth in 316–2 was the commercial state, without the hot deformation in Section 3.1. This means that the initial conditions were different for 316–1 and 316–2, so that their quantitative values in *Table* 5 are not comparable. A third series of experiments was conducted on Ni-30Fe. In that one, the samples were again subjected to the deformation process described in Section 3.1 at 900 °C, and then to annealing for times exceeding those required for full recrystallization. The initial condition for Ni-%30Fe was thus the recrystallized state in Fig. 5(b). In the first and third series, more grain growth is expected for longer annealing. This is confirmed by the increase of d_{RX} with longer time in the table. For 316–2, greater grain growth is expected for higher temperature, following the thermal activation of the process. *Table* 5 indicates that this was also the case. Microstructures corresponding to the second set of experiments (316–2) can be seen in Fig. 8. Fig. 9 contains microstructures for the third set of experiments, conducted on Ni-30Fe.

Table 5 shows that p monotonically decreased during grain growth, for all three sets of experiments. This is the same observation as in previous studies on annealing twinning [1,17,33,57–61]. Likewise, Table 5 generally indicates a monotonic decrease of n. This happened for all the sets of experiments but for the second, where n remained unchanged. Nevertheless, this was probably only because the difference in annealing times was too small for the effect to emerge (i.e., 12 s against at least 100 s in the third set). The decrease of n during grain growth is also the general observation in the annealing twinning literature [17,57,59].

Going further, p is discretized in Table 5 into the individual densities of Σ3 and Σ9 boundaries. The table indicates that the decay in the density of Σ9 boundaries during grain growth was much stronger than that of Σ3 boundaries, for all three series of experiments. For this to be more apparent, a column has been added to the table, indicating the magnitude of the decrease Δp relative to the density p of each twin boundary type in the base condition of each experiment set. The stronger decrease for Σ9 is clearly visible even for the relatively short annealing times in the second series of experiments. These results contrast with the view expressed by Bozzolo and Bernacki after their quasi in situ experiments, performed on 304 L stainless steel (SFE ≈ 25 mJ/m^2 [29,31]) [12]. Particularly, the authors pointed at twins comprising Σ9 boundaries being the most stable [12]. Yet, this view was based on two observed grains only [12]. What is more, quasi in situ experiments examine material behavior on its free surface, which may be different from that in the bulk. In this sense, the present results distinctly point at Σ9 boundaries predominantly being more unstable than Σ3 boundaries during grain growth, and in the bulk. The stronger decrease for Σ9 boundaries was such even if the increase in the density of Σ3 and Σ9 boundaries upon recrystallization occurred at essentially the same pace.

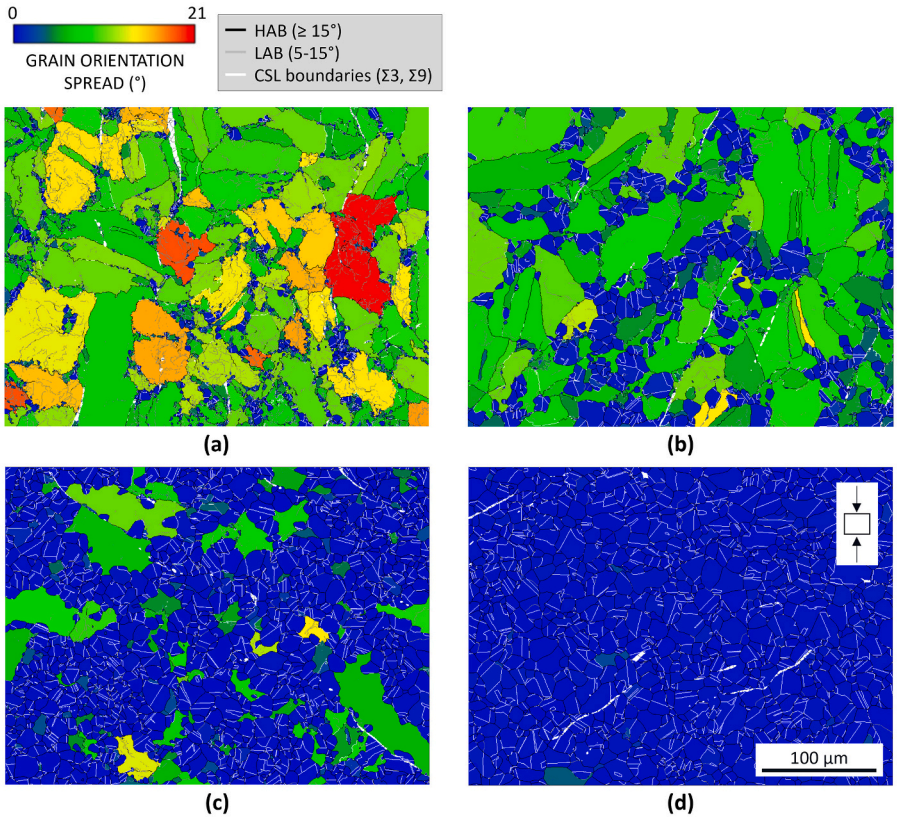

Fig. 4. Microstructures of 316 L-1 after deformation and annealing for different times: (a) 0.5 s, (b) 6.5 s, (c) 12 s, and (d) 24 s. The colour scale represents the grain orientation spread (GOS) values, with blue colors corresponding to recrystallized grains. The white colour accounts for pixels indexed as BCC. (For interpretation of the references to colour in this figure legend, the reader is referred to the web version of this article.)

This is illustrated in Fig. 10 for Ni-30Fe deformed and annealed at 900 °C. The figure displays that the evolution of Σ3 and Σ9 boundaries did not differ before 100 s (f_{RX} = 0–97 %), but only after 100 s ($f_{RX} \geq 97$ %, i.e. when only grain growth is active).

3.4. Annealing twin statistics in microstructures reconstructed from martensite

For the carbon steel, the results were obtained by EBSD reconstruction of the parent austenite from the martensite phase in which the steel was present after quenching. The recrystallization and twinning statistics in these reconstructed microstructures are shown in Table 6. Results are given for two different deformation conditions, varying in applied strain (0.2 and 0.4). Deformation temperature and strain rate were equal in both cases (950 °C and 10 s^{-1}). For each deformation condition, three annealing times were examined: 0.5 s (i.e., quenching immediately after deformation), 20 s (when recrystallization is nearly finished, or has just finished) and 500 s (when the material has sustained significant grain growth after the end of recrystallization). Examples of the reconstructed microstructures are displayed in Fig. 11.

Table 6 indicates that, as expected [21,52,53,56], higher applied strain accelerated recrystallization (i.e., recrystallized fraction was higher for the same annealing time), and reduced the recrystallized grain size. This ability of EBSD parent austenite reconstruction methods to capture recrystallized fraction and grain size trends was already demonstrated by former research [34]. Regarding the twinning statistics, Table 6 shows that, for the strain of 0.2, n substantially increased from 0.5 to 20 s. At the same time, the recrystallized fraction increased considerably, from ~50 to ~90 %. This agrees with the monotonic increase of n during recrystallization, reported by Jin et al. for pure nickel deformed at room temperature [1,7], and also observed here for 316 L-1 and Ni-30Fe (Section 3.1). In contrast, for the strain of 0.4, n stayed roughly constant between the same annealing times. In that case, the recrystallized fraction merely grew from ~90 to 100 %. This behavior is thus similar to the stagnation of n described for 316 L-1 and Ni-30Fe in Section 3.1. Afterwards, n decreased significantly between 20 and 500 s for both strains (Table 6). This is the expected behavior during grain growth, as noted in Section 3.3. About p, for the same recrystallized fraction near the end of recrystallization (~90 %, after 20 s for the strain of 0.2, and after 0.5 s for the strain of 0.4), its value decreased with lower applied strain (Table 6). This is also the effect of applied strain on annealing twin density usually found in the literature (see Section 3.2).

In addition, the micrographs in Fig. 11 give information on the boundary character of the reconstructed annealing twin boundaries. In those figures, recrystallized and deformed grains are shown in different colors, based on their different GOS values. Inside the recrystallized grains, CSL character was effectively detected for all the twins. Moreover, in the same way as for the materials directly scanned in austenite phase (Fig. 4 and Fig. 5), that CSL character could be observed along the whole length of the twin boundaries (see white lines inside the blue grains of Fig. 11). By contrast, for the twin boundaries inside the deformed grains, CSL character was in general not detected (e.g., orange arrows in Fig. 11(a)). At most, for a few of those twin boundaries, CSL character existed along a fraction of their length (e.g., green arrows in Fig. 11(a)). Similar behavior was also observed for the materials scanned as austenite (e.g., orange and green arrows in Fig. 5(d)). For both the reconstructed maps and those directly obtained from room-temperature austenite, a deviation compared to the theoretical CSL misorientation was allowed in the identification of twin boundaries, determined by Brandon's criterion [48]. The absence of CSL character for annealing twin boundaries in deformed grains is a general observation for FCC metals [23,62–64]. The reason is the crystallographic rotation that

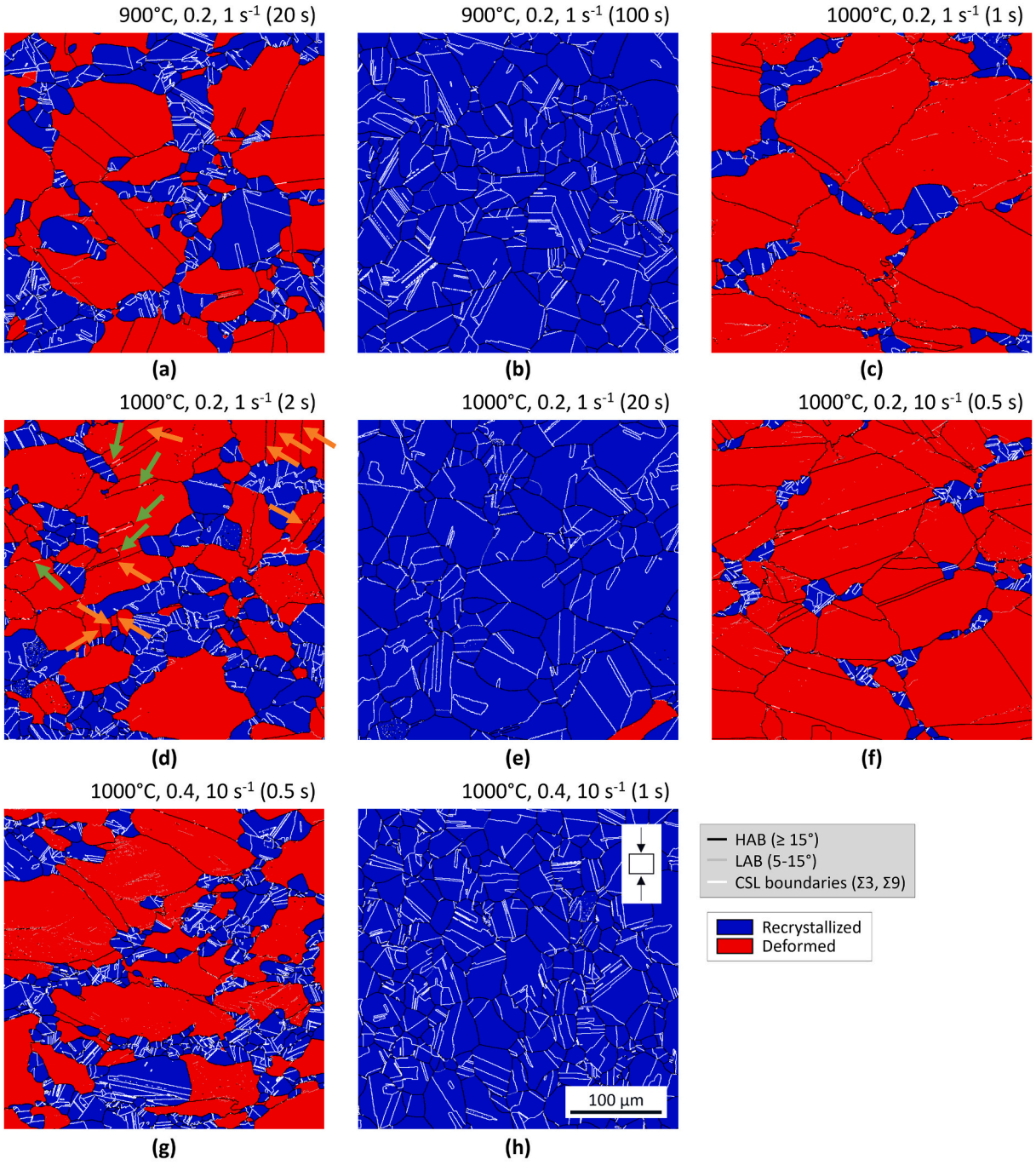

Fig. 5. Cropped fragments of the EBSD maps analyzed for Ni-30Fe deformed in different conditions, and then annealed for different times: (a) 900 °C-0.2-1 s^{-1} and 20 s, (b) 900 °C-0.2-1 s^{-1} and 100 s, (c) 1000 °C-0.2-1 s^{-1} and 1 s, (d) 1000 °C-0.2-1 s^{-1} and 2 s, (e) 1000 °C-0.2-1 s^{-1} and 20 s, (f) 1000 °C-0.2-10s^{-1} and 0.5 s, (g) 1000 °C-0.4-10s^{-1} and 0.5 s, and (h) 1000 °C-0.4-10s^{-1} and 1 s. Deformed and recrystallized grains are shown in red and blue, respectively, as separated based on grain orientation spread (GOS). The arrows in (d) point at former twin boundaries (FTBs) inside deformed grains: orange and green arrows indicate examples of FTBs having totally and partially lost their CSL characters, respectively. (For interpretation of the references to colour in this figure legend, the reader is referred to the web version of this article.)

accompanies plastic deformation: twins rotate differently from their parent grains. That rotation leads twin boundaries to gradually deviate from their CSL misorientations [23,62–64], with which they form during annealing, and which they thus possess at the start of deformation. In fact, due to this effect, twin boundaries inside deformed grains have been referred to as former twin boundaries (FTBs) [23].

4. Discussion

In Section 4, the effects of grain growth (Section 4.1) and recrystallization (Section 4.2) on annealing twin development are successively discussed, as generally observed in Section 3 for the case of hot-deformed austenite in steels. Afterwards, the suitability of EBSD parent austenite reconstruction methods to study annealing twinning in steels which undergo phase transformation upon cooling is explained in Section 4.3. Finally, the reasons for the different twin densities after

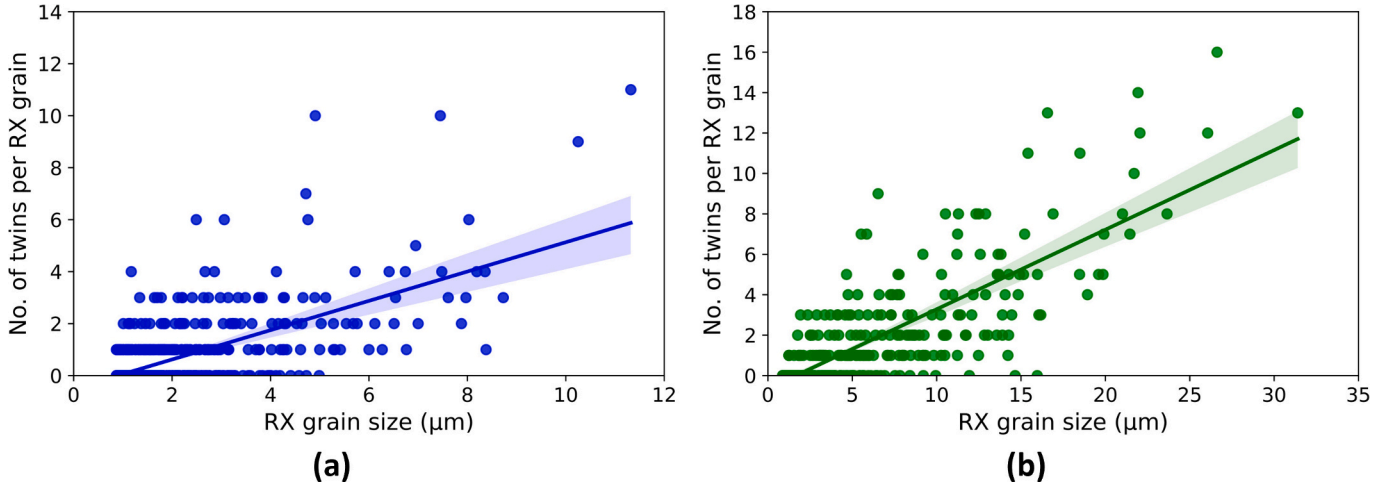

Fig. 6. Number of twin boundaries per recrystallized (RX) grain as a function of grain size for all the individual recrystallized grains identified in 316 L-1 after annealing for (a) 0.5 s, and (b) 6.5 s. The solid lines account for linear regression fits. The shaded area surrounding the lines represents a confidence interval for the fit, with a confidence index of 95 %.

Table 3
Summary of statistics at the end of recrystallization after deformation under different conditions for 316 L-1 and the Ni-30Fe alloy: recrystallized grain size d_{RX} and fraction f_{RX}, number of twin boundaries per recrystallized grain n, and annealing twin density p.

Alloy (condition)	Annealing time (s)	f_{RX} (%)	d_{RX} (μm)	n	p (mm^{-1})
316 L-1 (1000 °C-0.4-1 s^{-1})	24	99	10.4	0.81	65.2
Ni-30Fe (900 °C-0.2-1 s^{-1})	100	97	36.4	1.03	56.3
Ni-30Fe (1000 °C-0.2-1 s^{-1})	20	96	39.5	0.99	45.6
Ni-30Fe (1000 °C-0.4-10s^{-1})	1	100	28.5	1.03	65.0

Table 4
Summary of statistics for the Ni-30Fe alloy annealed to a recrystallized fraction f_{RX} of ~10 % after being deformed with different strain rates and temperatures: recrystallized grain size d_{RX} and fraction f_{RX}, number of twin boundaries per recrystallized grain n, and annealing twin density p.

Alloy (condition)	Annealing time (s)	f_{RX} (%)	d_{RX} (μm)	n	p (mm^{-1})
Ni-30Fe (900 °C-0.2-1 s^{-1})	10	11	12.1	0.90	116.9
Ni-30Fe (1000 °C-0.2-1 s^{-1})	1	10	10.9	0.51	81.0
Ni-30Fe (1000 °C-0.2-10s^{-1})	0.5	10	10.1	0.84	142.0

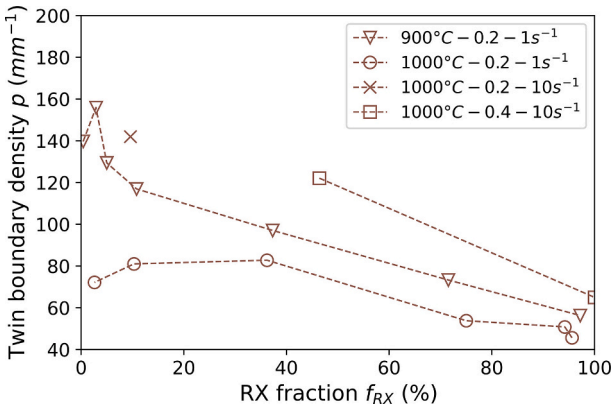

Fig. 7. Evolution of the density of annealing twin boundaries in the recrystallized grains p, as a function of the recrystallized (RX) fraction f_{RX}, for the different deformation conditions analyzed for the Ni-30 %Fe alloy.

recrystallization are discussed in Section 4.4, and rationalized via parameters related to the microstructures in the deformed state.

4.1. The effect of grain growth on annealing twinning

For the three grades examined, this study has shown that, when grain growth happens in the absence of simultaneous recrystallization, both the annealing twin density p and the number of annealing twins per grain n diminish (Table 5 and Table 6). Hence, those tendencies can be concluded to be intrinsic to hot-deformed austenite. Furthermore, for both parameters, such tendencies have also been observed in other FCC metals [1,6,17,33,57–61]. Yet, the mechanisms whereby n and p decrease during grain growth have been revealed only recently. Particularly, recent in-situ 3D-XRD [65] and quasi in situ EBSD experiments [1,12] have displayed that the number of twins forming during grain growth is negligible, compared to the number of those that are annihilated. If twins are annihilated without (a significant number of) new twins created, p and n can only naturally decrease. Additionally, the quasi in situ EBSD studies have identified two mechanisms whereby annealing twins disappear during grain growth. Firstly, relatively large grains containing fewer twins grow at the expense of relatively small grains that contain more twins [1]. Secondly, the incoherent segments of Σ3 boundaries migrate inside the grains, so that they collapse and disappear into the parent grain boundaries [12].

Both mechanisms are now applied to understand the more rapid decay in the density of Σ9 boundaries upon grain growth compared to Σ3 boundaries, observed in the present study. Again, such behavior was exhibited by both 316 L and Ni-30Fe (Table 5). This indicates that the behavior is intrinsic to, at least, hot-deformed austenite. For the carbon steel, Σ9 boundary density evolution could not be checked, owing to the insufficient number of boundaries present of that type. For the two mechanisms, the driving force for the elimination of the twin boundary is the same: the boundary energy of the twin. Therefore, considering either mechanism, that elimination is more likely for higher energy of the twin boundary. In this respect, Olmsted et al. calculated the interface energies [66] of a number of different boundaries in pure nickel, using

Table 5
Evolution of the density of Σ3 and Σ9 boundaries p during grain growth, for different sets of experiments corresponding to 316 L-1, 316 L-2 and the Ni-30Fe alloy. The average number of twin boundaries per grain n is also provided, together with the average grain size d_{RX} after each experiment. The decrease in p with respect to the base experiment for each set is also indicated. The data correspond to microstructures with a recrystallized fraction of at least 97 %.

Alloy	Annealing temperature (°C)	Annealing time (s)	d_{RX} (μm)	n	∑3 boundaries		∑9 boundaries	
					p (mm^{-1})	$\Delta p/p$	p (mm^{-1})	$\Delta p/p$
316 L-1	1000	24	10.4	0.81	63.0	–	2.3	–
		36	11.7	0.81	60.1	**−5 %**	1.6	**−30%**
316 L-2	900	300	39.1	1.79	42.6	–	3.2	–
	1100		40.1	1.39	32.3	**−24 %**	1.8	**−44 %**
	1150		45.8	1.12	21.4	**−50 %**	1.0	**−69 %**
Ni − 30%Fe	900	100	36.4	1.03	53.0	–	2.2	–
		200	45.8	0.98	37.2	**-30%**	1.1	**−50 %**
		1000	47.1	0.93	29.6	**−44 %**	0.8	**−64 %**

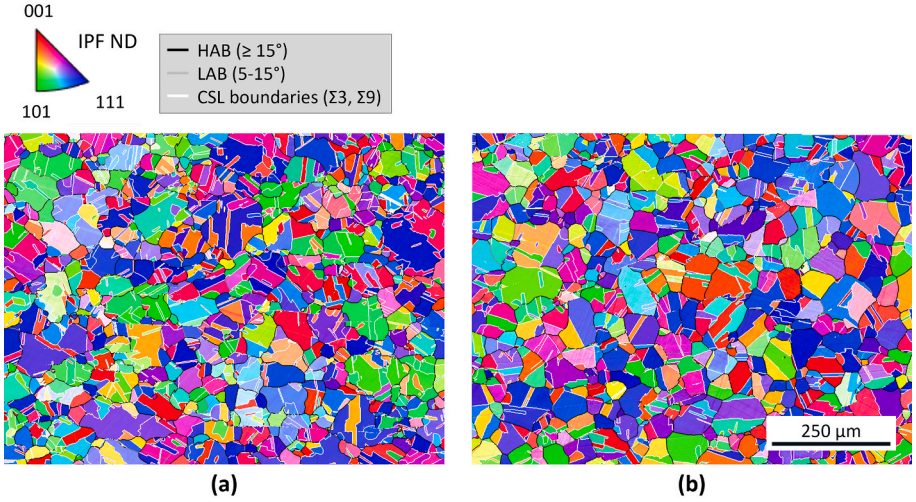

Fig. 8. Microstructures of 316 L-2 after soaking for 60 s at (a) 900 °C, and (b) 1100 °C. The map colors account for inverse pole figure (IPF) coding, parallel to the normal direction (ND) of sheet. The white colour accounts for pixels indexed as BCC.

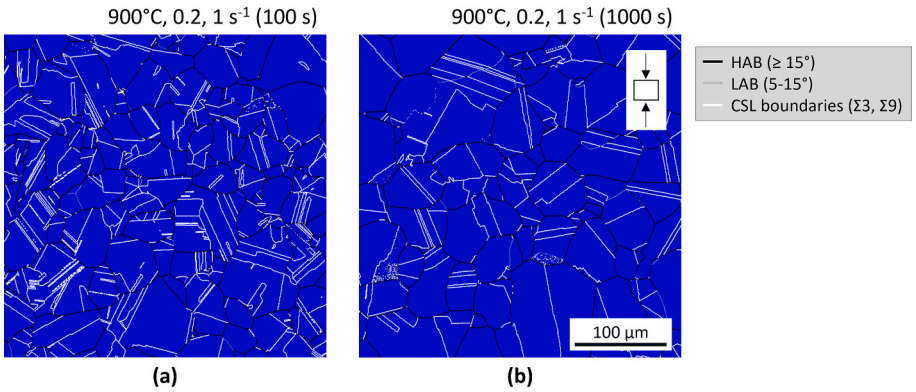

Fig. 9. Microstructures of the Ni-30Fe alloy deformed at 900 °C and annealed for (a) 100 s, and (b) 1000 s. Deformed and recrystallized grains are shown in red and blue, respectively. (For interpretation of the references to colour in this figure legend, the reader is referred to the web version of this article.)

molecular dynamics. The authors concluded that the energies of Σ9 boundaries are always higher than those of Σ3 boundaries, regardless of the coherency of Σ3 boundaries [66,67]. Hence, boundary energies can explain why Σ9 boundaries disappear more quickly than Σ3 boundaries. Besides, from the viewpoint of the kinetics, the first mechanism (preferential consumption of grains with more twins [1]) depends on the mobilities of the migrating parent grain boundaries. In turn, this does not depend on the type of twin boundary to be removed. By contrast, with the second mechanism [12], it is the twin boundary itself that migrates. Therefore, the relevant mobility is that of the twin boundary. Again through molecular dynamics, Olmsted et al. also investigated the interface mobilities of a wide range of boundaries in pure nickel [27]. The study suggested much lower mobility for coherent Σ3 boundaries than for Σ9 boundaries, albeit significantly higher for incoherent Σ3 boundaries [27]. Coherent Σ3 boundaries have been found to be much more profuse after recrystallization than incoherent Σ3 boundaries in both Ni-30Fe [26] and 304 L [12]. Hence, it is the lower mobility of the coherent Σ3 boundaries that is relevant when comparing the average behavior of Σ3 and Σ9 boundaries. Consequently, the higher mobility of Σ9 boundaries is expected to have also contributed to their quicker

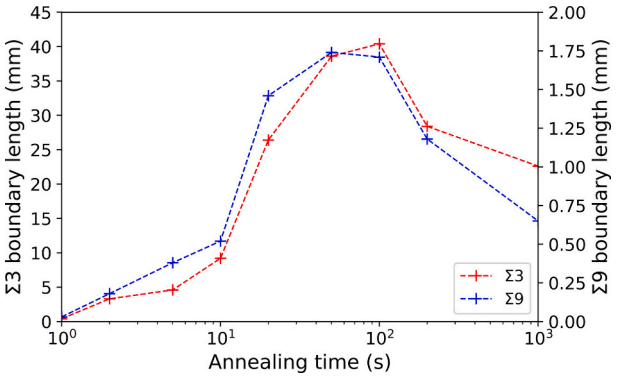

Fig. 10. Evolution of the density of Σ3 and Σ9 boundaries for the Ni-30Fe alloy, in the annealing experiments performed after deformation at 900 °C. For each annealing time, the densities have been calculated as the ratio between the total length of each boundary type L_{tb} in the recrystallized grains captured, and the total area analyzed by EBSD.

Table 6
Summary of statistics for the carbon steel after deformation under different conditions followed by annealing for different times: recrystallized grain size d_{RX} and recrystallized fraction f_{RX}, number of twin boundaries per recrystallized grain n, and annealing twin density p. The statistics were obtained after reconstruction of the parent austenite microstructure.

Alloy (condition)	Annealing time (s)	f_{RX} (%)	d_{RX} (μm)	n	p (mm^{-1})
Carbon steel (950 °C-0.2-10s^{-1})	0.5	47	26.7	1.04	455.8
	20	90	34.2	1.29	250.4
	500	100	28.8	0.80	198.8
Carbon steel (950 °C-0.4-10s^{-1})	0.5	87	15.4	0.66	366.7
	20	99	17.6	0.65	277.8
	500	100	21.7	0.53	72.0

elimination upon grain growth than Σ3 boundaries, in addition to their higher boundary energy.

4.2. The formation of twins during recrystallization

The results in this study have shown that, for the three analyzed materials, n increases gradually during recrystallization (Fig. 1(b), Fig. 2(b), Fig. 3(b) and Table 6, between 0.5 and 20 s for the strain of 0.2). Therefore, they indicate that twin boundaries are generally created in the recrystallization of hot-deformed austenite in steels. This agrees with the suggestion by Jin et al. for recrystallization of pure nickel deformed at room temperature [1,7]. Specifically, Fig. 6 displayed that the twin boundaries appear through the growth of the recrystallizing grains. Such a behavior agrees with the widespread 'growth accident' theory [3–7] to explain the formation of annealing twins. Additionally, the plots in Fig. 6 demonstrate that no minimum grain size is required for annealing twin formation to be activated: the number of twin boundaries increases with grain size starting from the smallest sizes, with twins regularly observed for grains smaller than e.g. 5 μm (Fig. 6(a)-(b)). This does not occur for e.g. deformation twins in hexagonal close-packed metals. For those, small grain sizes (i.e., below approximately 30 μm [68]) preclude twinning [68,69].

Nevertheless, also for the three analyzed materials, the increase of n during recrystallization stagnated before the end of recrystallization (Fig. 1(b), Fig. 2(b), Fig. 3(b) and Table 6, see n after 0.5 and 20 s for the strain of 0.4). This was not the case for pure nickel deformed at room temperature, and then annealed at low temperature: n increased linearly across the whole recrystallization process, including recrystallized fractions higher than 95 % [1,7]. For the materials here studied, the stagnation started well before that: at recrystallized fractions of ~80 % for 316 L-1, ~40 % for Ni-30Fe and, at most, 87 % for the carbon steel (Table 6). This similarity for the three materials implies that the stagnation of n is intrinsic to austenite in steels, deformed and annealed at high temperature.

The explanation to this distinct behavior of hot-deformed austenite can be found in the evolution of the density of recrystallized grains N_{RX} during recrystallization. This is shown for 316–1 in Fig. 1(c), and for the two recrystallization routes examined for Ni-30Fe in Fig. 2(c) and Fig. 3(c). The plots indicate that N_{RX} did not increase monotonically throughout recrystallization. On the contrary, N_{RX} increased steadily in the earlier stages, but then decayed after certain point, also steadily. This reduction in N_{RX} can be explained by grain growth simultaneous to recrystallization. In recrystallization, recrystallized grains grow at the expense of deformed grains. In grain growth, by contrast, they consume other recrystallized grains. This can effectively decrease the overall number of recrystallized grains in the microstructure. In fact, grain growth concomitant to recrystallization has often been reported in studies on the annealing of hot-deformed austenite in steels [52,53]. In the present case, the onset of the decay in N_{RX} approximately coincided with the stagnation of n for the three recrystallization processes (Fig. 1(b), Fig. 2(b) and Fig. 3(b)). As discussed in Section 4.1, grain growth reduces the density of annealing twins. Therefore, if grain growth begins before recrystallization is complete, as in the present case, its onset can lead to the stagnation of n upon recrystallization: a balance may be reached between the creation of twin boundaries via recrystallization, and the elimination of others by grain growth. This is confirmed for the annealing of hot-deformed austenite by the behavior of Ni-30Fe at 900 °C, for which annealing times considerably longer than needed for full recrystallization are included in the plots (Fig. 2(b)): when both grain growth and recrystallization occurred ($d_{RX} \approx$ 18–36 μm), n remained roughly constant; when recrystallization was complete, and only grain growth was thus active ($d_{RX} >$ 36 μm), n started to slowly decrease (as explained in Section 4.1). Grain growth simultaneous to recrystallization also explains the stagnation of n for the carbon steel, when this was observed: after the strain of 0.4, N_{RX} decreased from 7430 grains/mm^2 to 5920 grains/mm^2 (Table 6).

In addition, simultaneous recrystallization and grain growth leading to the stagnation of n also explains the absence of stagnation in the recrystallization of pure nickel deformed at room temperature: Jin et al. reported that, in their case, grain growth and the associated decrease in N_{RX} began only after the end of recrystallization [1,7]. This lack of grain growth concomitant to recrystallization in [1,7] can be explained by the considerably lower annealing temperatures, ranging between 350 and 450 °C [1,7]. Grain growth concomitant to recrystallization is more likely for higher annealing temperature, due to the increasing HAB mobility [52,53]. Similarly, the retardation in the prevalence of grain growth (and, thus, of the stagnation of n) for 316 L-1 compared to Ni-30Fe (for the deformation conditions that employed 1 s^{-1} for this alloy) can be ascribed to the higher strain rate used for 316–1. In the recrystallization of hot-deformed austenite, increasing the strain rate within the 1–10 s^{-1} range has been found to considerably enhance the nucleation of new grains [54,55]. This enhancement of nucleation can delay the prevalence of grain growth simultaneous to recrystallization, by extending the regime where new recrystallized grains are produced into longer annealing times.

Finally, it remains to be explained why the density of Σ3 and Σ9 boundaries increases in such a similar way upon recrystallization (Fig. 10). In FCC microstructures, Σ3 boundaries form by 'growth accidents', while Σ9 boundaries form when two Σ3 boundaries encounter [8]. The density of either boundary type will increase when: (i) a new twin boundary of that type forms, or (ii) a pre-existing twin boundary of that type extends in length as its parent grain grows [1]. Following either effect, an increase in the density of Σ3 and Σ9 boundaries at the same rate is only reasonable: (i) the chance that Σ3 boundaries meet (and, thus, a Σ9 boundary forms) is higher when more Σ3 boundaries exist in the microstructure; (ii) the rate at which twin boundaries extend

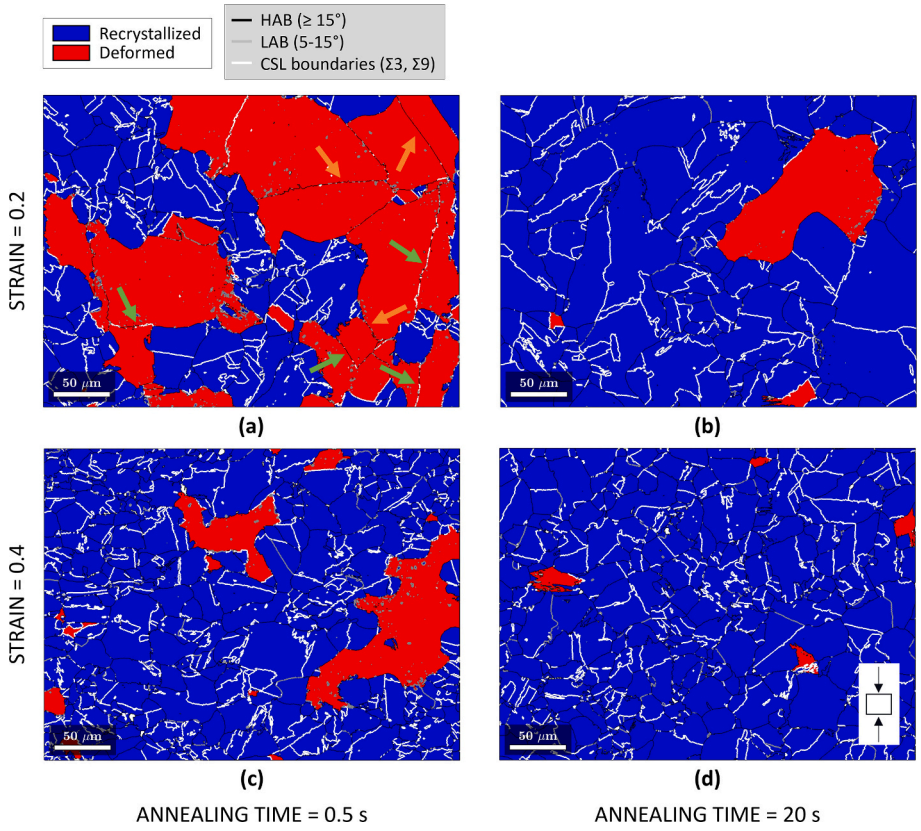

Fig. 11. Fragments of the microstructures analyzed for the carbon steel deformed at a strain of (a, b) 0.2 and (c, d) 0.4, and annealed for (a, c) 0.5 s and (b, d) 20 s. The deformed and recrystallized grains have been separated (red and blue, respectively) on the basis of grain orientation spread (GOS), after reconstruction of the parent austenite microstructure. The arrows in (a) point at former twin boundaries (FTBs) inside deformed grains: orange and green arrows indicate FTBs having totally and partially lost their CSL characters, respectively. (For interpretation of the references to colour in this figure legend, the reader is referred to the web version of this article.)

depends on the migration velocity of the parent grain boundary. That velocity is widely accepted to be dictated by the stored energy ahead of the migrating boundary [2], i.e. to be independent of the particular type of any neighboring twin boundary.

In conclusion, like for the cases previously studied in the literature, annealing twins in hot-deformed and annealed austenite in steels are created by recrystallization, and tend to disappear by subsequent grain growth. Particularly, twin boundaries have been shown to form by the growth of the recrystallized grains into the deformed microstructure, in agreement with the 'growth accident' theory. However, unlike in the previously investigated cases, the number of twins per recrystallized grain stops increasing well before the end of recrystallization. This is due to the effect of grain growth starting while recrystallization is still in progress, which does not happen for lower annealing temperatures.

4.3. Suitability of parent austenite reconstruction to study annealing twinning

In Sections 4.1 and 4.2, it was noted that the behavior of the carbon steel as examined via EBSD parent austenite reconstruction did not qualitatively differ from that of 316 L and Ni-30Fe: n monotonically increased during recrystallization until the onset of grain growth, which led to the stagnation of n and its subsequent reduction once recrystallization was complete; likewise, p monotonically decreased during recrystallization. 316 L and Ni-30Fe could be investigated without any reconstruction. Hence, it can be concluded that the employed parent austenite reconstruction method captured all the correct tendencies concerning annealing twin statistics. This suggests that this methodology can be used to study not only aspects of recrystallization such as kinetics and texture evolution [34], but also annealing twin behavior. Furthermore, the micrographs in Fig. 11 showed that parent austenite reconstruction allows for a good representation of the original CSL character of twin boundaries, and its loss upon plastic deformation (see Section 3.4).

Nevertheless, the question remains as to whether the specific values arising from the reconstruction are realistic: the twin densities p shown in Table 6 for the carbon steel are much higher than those measured for either 316 L or Ni-30Fe (Table 3 and Table 4). On the other hand, SFE is similar for the carbon steel and Ni-30Fe [28]. Consequently, their intrinsic tendencies for twinning should not significantly differ. The smaller grain size before deformation (~50 μm against ~90 μm) considered for the carbon steel may partly account for the discrepancy: Jin et al. found a considerable increase of p when reducing the initial grain size in their study on pure nickel [7]. However, the role of reconstruction artifacts affecting annealing twin boundary lengths should also be considered.

Specifically, it is well-known that two parent grains related by a CSL Σ3 type misorientation have each six martensitic variant orientations that are crystallographically similar to each other [35]. These variants all belong to a single packet sharing the same habit plane, which for the shared variants is the habit plane closest to the {111} boundary plane of the coherent CSL Σ3 boundary. This means that variants with identical or close-to-identical crystallographic orientations may form on both sides of the twin boundary. Experimentally, this has been observed to frequently be the case [35]. Furthermore, martensite in low-alloy carbon steel consists of a block structure within the packets, with each block consisting of pairs of variants with crystallographically close-together orientations. Thus, both the identification of singular martensitic laths

and the distinction of laths across a twinning boundary may be impossible when a simple misorientation angle threshold is used to distinguish martensitic sub-units from each other in an orientation map. This makes the accurate reconstruction of annealing twin boundaries particularly difficult.

The aforementioned problems (i.e., the distinction of variants at and in the vicinity of the twin boundaries) result in zigzag annealing twin boundaries. An example of this is shown in Fig. 12 for the present carbon steel, in the sample deformed to a strain of 0.2 and annealed for 20 s. Particularly, the parent austenite grains (each encompassing several annealing twins) have smooth boundaries (shown with thick black lines), with a morphology consistent with the expectations for equiaxed grains. In contrast, the CSL Σ3 annealing twin boundaries (shown with cyan lines) have in many cases zigzagging, serrated features that are not consistent with the expectation: CSL Σ3 boundaries should, for the most part, follow the trace of the {111} boundary plane. A distinct case of zigzag boundaries is highlighted with a red rectangle in Fig. 12(a)-(b). A closer inspection of the corresponding structure in the martensite orientation map (with thin black lines showing the martensite boundaries) in Fig. 12(c) sheds light on the reason for such zigzag boundaries: the chaotic area is encompassed by a large, irregularly shaped martensitic sub-unit (the pink colored grains). The shape of this sub-unit indicates that several singular laths have been mistakenly merged into a single sub-unit during the initial grain construction step of the parent reconstruction algorithm. The orientations of the laths have been similar enough that even the use of the relatively strict 2° misorientation angle threshold has not been sufficient to determine the structure. The presence of annealing twin boundaries in the neighborhood of this large sub-unit indicates that martensitic variant orientations across the actual annealing twin boundary have been merged together. Since unique parent orientation solutions are determined for each sub-unit by the variant graph algorithm, it is naturally impossible to correctly identify the twin boundaries in this situation. Other annealing twin boundaries in the map have a more regular appearance; in these cases, variants with significantly different orientations had formed both at and in the vicinity of the twin boundaries.

Following this zigzag nature of some of the reconstructed twin boundaries, it is likely that the measured twin boundary lengths overshoot the true values. This can partly explain the particularly high annealing twin densities p here found for the carbon steel. Further research is thus needed to elucidate if the specific annealing twin densities offered by parent austenite reconstruction methods are generally realistic. Nevertheless, it is highly encouraging that reconstructed parent austenite maps can capture similar general behavior and trends as directly measured maps. Moreover, the zigzag effect should not affect the specific n values measured: n depends on the number of twin boundaries in the microstructure, and not on their lengths. In fact, the n values measured for the carbon steel (Table 6) are reasonable, and in the same range as those found for 316 L and Ni-30Fe (Table 3 and Table 4).

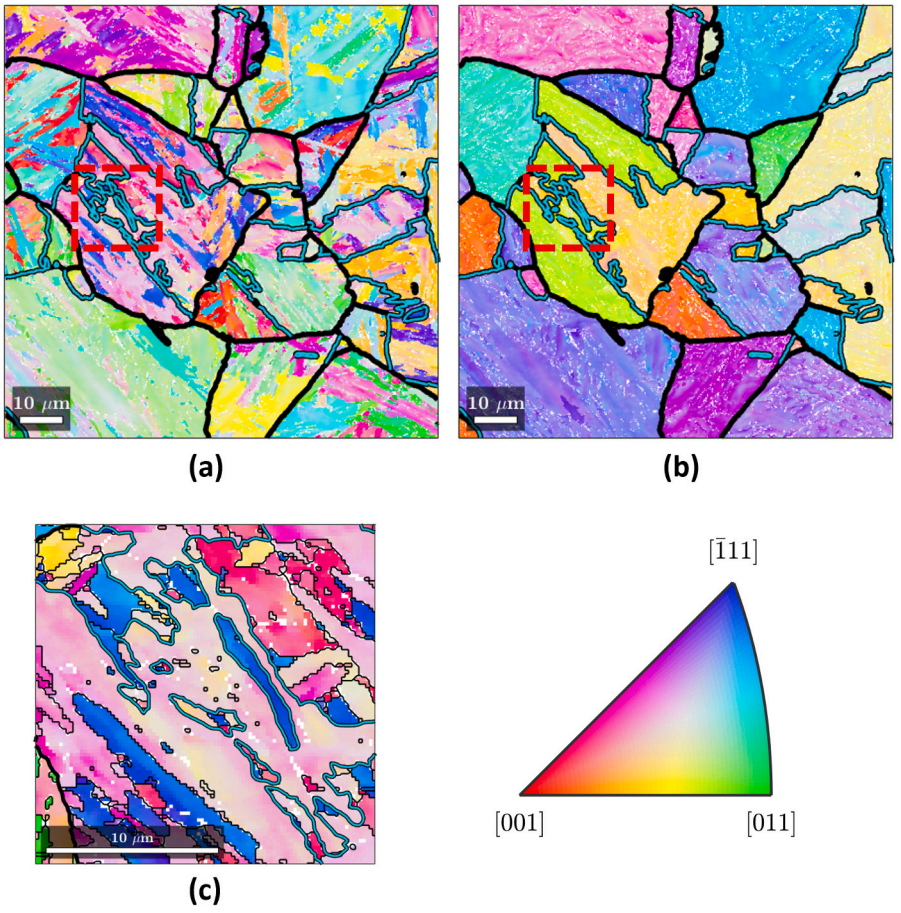

Fig. 12. Cropped fragment of (a) the child orientation and (b) the reconstructed parent orientation maps corresponding to the specimen compressed to an applied strain of 0.2 at a strain rate of 10 s-1 and 950 °C, followed by annealing for 20 s. Parent austenite grain boundaries are shown in black, while CSL Σ3 boundaries have been highlighted cyan. The orientations are colored with inverse pole figure (IPF) Z coloring, with Z referring to the imaging plane normal. (c) displays the cropped fragment indicated by a red rectangle in (a) and (b). In (c), the martensite boundaries are indicated with thinner black lines. (For interpretation of the references to colour in this figure legend, the reader is referred to the web version of this article.)

4.4. Factors behind the annealing twin density variations among deformation conditions

Like for other materials [3,5,7,33], the results in Section 3.2 revealed that, for hot-deformed austenite, different deformation conditions produce varying annealing twin densities p after recrystallization. Specifically, p increases with lower annealing temperature, higher strain rate and higher applied strain. In this section, such variations are rationalized through parameters describing the deformed microstructures resulting from different conditions. This is particularly important: no parameter is widely accepted to date that can explain the effect of deformation conditions on annealing twin density, regardless of the material. In addition, the values of p in Section 3.2 implied a different tendency for twinning in 316 L and Ni-30Fe. The reason for this is briefly examined at the end of this section. The carbon steel is not included in the comparison because the values of p are affected by the parent austenite reconstruction, as explained in Section 4.3.

For the deformation conditions examined on Ni-30Fe, Table 7 displays the annealing twin density p measured after recrystallization, and two microstructural parameters describing the original deformed microstructure: the average dislocation density ρ_0 in the deformed grains of the sample quenched just after deformation, and the average tortuosity of the recrystallization front τ. About dislocation density, it provides a quantitative measure of the energy stored in a deformed microstructure, which drives recrystallization [2]. In the present case, ρ_0 increased with lower temperature of deformation (for the same strain and strain rate). ρ_0 also increased with higher applied strain and strain rate (for the same deformation temperature). In both cases, this is the expected trend [2].

About the average tortuosity of the recrystallization front τ, it accounts for how much the boundaries between recrystallizing and deformed grains deviate from a straight line. This parameter was successfully related to the twin boundary density p after recrystallization by Jin et al. [7]. In the present case, τ was derived via Eq. (3), following the same procedure as in [7], with the OIM Analysis 7.3 software. For each deformation condition, τ was calculated for an annealing time corresponding to an intermediate recrystallized fraction (Table 7). That was chosen as tortuosity is expected to be more easily detected well after nucleation, but also well before the final impingement of the recrystallizing grains. At the same time, the recrystallized fractions selected (~35–45 %, Table 7) lie all in the range where twin generation increased linearly with recrystallized fraction (see Fig. 2(b) and Fig. 3(b)). Moreover, the previous study considered similar recrystallized fractions (albeit with much greater variation among deformation conditions, i.e. ~45–80 % [7]). About the present τ values, Table 7 indicates that they followed a different trend compared to ρ_0. Firstly, τ decreased considerably with lower deformation/annealing temperature. This behavior agrees with the results by Suh et al., who reported a monotonic increase in the amplitude of the largest boundary serration in a partially recrystallized microstructure with higher temperature of deformation/annealing (for equal strain and strain rate) [70]. The study considered the same Ni-30Fe alloy as here, analogous hot compression tests, and a similar deformation condition range [70]. In this sense, the tortuous character of recrystallizing boundaries has been widely associated to contrasting growth rates into areas with locally higher and lower stored energy [7,71,72]. Hence, the increased boundary mobility expected at the higher temperature seems to have enhanced this difference in growth rates. In addition, the τ value in Table 7 decreased with higher applied strain and strain rate. This is also in line with Suh et al.: for the same temperature and strain rate, the amplitude of the largest serration in the microstructure saturated for strains higher than 0.2 [70] (i.e., the minimum strain in Table 7); at the same time, it decreased with increasing strain rate (for the same temperature and strain) [73]. Assuming the conclusions by Suh et al., increasing strain from 0.2 to 0.4 should have no effect on boundary tortuosity. In turn, increasing strain rate from 1 to 10 s^{-1} should reduce its value. This is observed in Table 7. Specifically, previous research has consistently suggested that dislocation boundaries constitute the areas with locally higher stored energies which drive the migration of the recrystallizing boundaries [7,71,72]. Therefore, the lack of variation of boundary tortuosity with higher strain suggests that subgrain size also saturates with increasing strain. Conversely, the smaller serrations for higher strain rate would be in line with a concomitant reduction of the subgrain size. Nevertheless, further research is needed to elucidate these two points. In any case, the present results do suggest that the trends observed by Suh et al. [70,73] apply also to the tortuosity of the recrystallizing boundaries on average, and not only to those exhibiting the largest serration.

However, in the present case, the annealing twin density p after recrystallization (Table 3) did not increase with the boundary tortuosity τ (Table 7). For instance, the condition with the highest τ exhibited the lowest p (1000 °C and strain of 0.2). These results mean that tortuosity cannot explain the twin density variations observed here. This is unlike the study by Jin et al., where a positive correlation was found between p and τ [7]. In this respect, a more tortuous boundary would be expected to contain more sections locally parallel to one of the {111} octahedral planes of the growing grain. The latter is a requisite for the formation of growth accidents [3,5]. Hence, more tortuous boundaries may produce more annealing twins [7]. Yet, the correlation between p and τ in the previous study was demonstrated for three deformation conditions only [7]. Moreover, the study dealt with pure nickel (a material with much higher SFE than Ni-30Fe or carbon steels [28]) deformed at room temperature, then annealed at 350–450 °C (i.e., much lower than the temperatures dealt with here) [7]. One difference with respect to the study by Jin et al. is the lack of grain growth concomitant to recrystallization in their case [1]. Grain growth simultaneous to recrystallization affects the resultant twin density by the elimination of twin boundaries as recrystallization proceeds. In turn, that could alter the correlation between p and τ. Nevertheless, Fig. 7 shows that the trends of p with deformation parameters held throughout the whole recrystallization process for all the examined conditions, including at the lowest recrystallized fractions. By contrast, grain growth would be expected to play a relevant role at later recrystallization stages only. Additionally, the velocity of the recrystallizing boundaries also fails to explain the variations of p. Previous research had considered this factor to explain contrasting twin densities after different processing conditions [1,6,32,33]. It was understood that growth accidents on a moving boundary are more probable for quicker migration rates [5]. However, p here was higher after deformation at 900 °C than at 1000 °C, for the same applied strain and strain rate (Table 3). This was despite considerably slower recrystallization at 900 °C (compare e.g. the annealing times required to reach the same recrystallized fractions in Table 3 and Table 7). Another discrepancy with the proposed role of boundary migration velocity had

Table 7
Average tortuosity of the recrystallization front τ measured after selected annealing times, and dislocation density ρ_0 measured immediately after deformation (annealing time ≈ 0.5 s), for the Ni-30Fe alloy deformed under three different conditions. The recrystallized grain size d_{RX} and fraction f_{RX}, the number of twin boundaries per recrystallized grain n, and the twin density p for the same annealing time as considered for τ are also displayed.

Alloy (condition)	Annealing time (s)	f_{RX} (%)	d_{RX} (μm)	n	p (mm^{-1})	τ	ρ_0 (m^{-2})
Ni-30Fe (900–0.2-1 s^{-1})	20	37	17.6	1.04	97.0	1.57	$5.2{\cdot}10^{14}$
Ni-30Fe (1000–0.2-1 s^{-1})	2	36	16.9	0.76	82.8	1.81	$4.6{\cdot}10^{14}$
Ni-30Fe (1000–0.4-10s^{-1})	0.5	46	13.2	0.95	122.1	1.64	$6.1{\cdot}10^{14}$

been encountered in [7]: p did not change when the same deformed microstructure was annealed at temperatures with markedly different recrystallization kinetics.

On the other hand, annealing twin density p did increase with higher dislocation density ρ_0 at the start of recrystallization (Table 7 and Fig. 13). This parameter has not usually been acknowledged for explaining variations in twin density. Nevertheless, Burke pointed out that growth accidents may be promoted by discontinuities within the consumed matrix like dislocation boundaries [3]. The density of such dislocation boundaries in a deformed microstructure is generally expected to increase with higher dislocation density. Consequently, that effect could explain the observed correlation between p and ρ_0. In fact, in situ EBSD experiments on a nickel superalloy have revealed that twin boundaries typically form upon the encounter of a migrating boundary with second-phase precipitates [74]. These also represent discontinuities in the deformed matrix. In turn, the generation of annealing twin boundaries at microstructural discontinuities might be explained by their effect on creating short-range roughness in the migrating boundaries of the recrystallized grains. This refers to roughness with a smaller amplitude than resolvable with the EBSD step sizes employed either here or in [7] (0.5 and 1.25 μm, respectively). For instance, dislocation boundaries are widely accepted to produce boundary roughness in the recrystallized grain boundaries, via the local enhancement of the growth rates of the boundary portions in contact with them [7,71,72]. Nevertheless, Beladi et al. found, using transmission electron microscopy, microband spacings between 0.2 and 1 μm after deformation of Ni-30Fe in similar conditions to those of this study (1000 °C, 1 s^{-1} and a strain of 0.3) [26]. Such spacings cannot be resolved with EBSD step sizes like those used here or in [7]. Yet, reducing the step size to the necessary level would imply a decrease in the area size analyzed, compromising the statistical representativity of results. Therefore, the correlation found here between p and ρ_0 may be explained by the enhancement of short-range boundary roughness with higher ρ_0. This would constitute a physical rationale for the role of microstructural discontinuities in producing annealing twin boundaries, suggested above.

Finally, Table 3 displayed the same annealing twin density p for 316 L and Ni-30Fe, despite the lower strain rate applied to the former. Since higher strain rate leads to a higher value of p, this suggests a greater intrinsic tendency for twinning in 316 L. In turn, this can be explained by its lower SFE: 25–35 mJ/m^2 [29–31], against ~75 mJ/m^2 [28] for Ni-30Fe. Lower SFEs in FCC metals have been widely related to stronger probabilities for annealing twin formation [6,8,11,24]. This agrees with the requirement for stacking faults to form assumed by the 'growth accident' theory. Similarly, the twin densities of Ni-30Fe after recrystallization (Table 3) can also be compared to those reported by Jin et al. for pure nickel. Particularly, lower values were measured for pure nickel (30–45 mm^{-1} [7], against 45–65 mm^{-1} in Table 3), for all the deformation conditions examined in either study. This was despite the much lower deformation temperature applied to pure nickel (room temperature), and the higher strains (30 % and 60 %) [7]. Nevertheless, the lower values of p for pure nickel can be explained by its higher SFE: ~120 mJ/m^2 [28], against ~75 mJ/m^2 [28] for Ni-30Fe. The initial grain size before deformation was of approximately 90 μm for both Ni-30Fe and pure nickel [7]. As a result, this variable is not expected to have played a role.

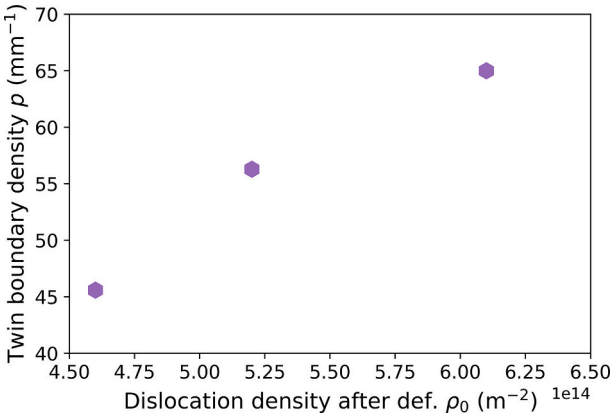

Fig. 13. Twin boundary density p at the end of recrystallization (Table 3) for the various deformation conditions studied on the Ni-30Fe alloy, as a function of the dislocation density ρ_0 measured immediately after deformation (annealing time ≈ 0.5 s).

To sum up, the initial dislocation density (i.e., stored energy) in the deformed microstructure is proposed here as a factor to explain the observed variations in annealing twin boundary density after recrystallization. Therefore, the further exploration of the correlation between both variables in future research is advisable. Moreover, understanding the origin of annealing twinning in FCC metals requires a better understanding of the interactions between migrating boundaries and microstructural obstacles. This includes their effect on boundary topology and roughness. Despite this, it should also be considered that dislocation density can satisfactorily account for the annealing twin density trends found not only in the present study, but also in the previous ones. Particularly, the recurrent observations of twin density enhancement with stronger prior plastic deformation [3,5,7,33] are well explained by the higher dislocation densities that should also result. Furthermore, dislocation density holds also for all the deformation/annealing parameters studied by Jin et al.: like higher applied strain, the authors found smaller initial grain size to increase twin density [7]. Both are known to generally lead to higher stored energies after deformation [2]. The lack of impact of annealing temperature for the same deformed microstructure [7] also agrees with the dislocation density imparted by deformation being the factor that determines annealing twin density.

5. Conclusions

The development of twinning in hot-deformed austenite in steels during annealing has been here studied for the first time. Particularly, one stainless steel, one carbon steel, and a Ni-30Fe alloy have been examined. These are the main conclusions:

1. Annealing twin boundaries are created by recrystallization, and disappear via grain growth. Yet, unlike previously observed for low temperature annealing in pure nickel, the number of twin boundaries per recrystallized grain does not increase throughout the recrystallization process. On the contrary, that number stagnates once the density of recrystallized grains starts decreasing. This is due to grain growth initiating before recrystallization ends, which does not occur at lower annealing temperatures. After recrystallization is complete, the number of twins per grain simply decreases via grain growth.
2. Twin boundary density after recrystallization is higher for lower deformation temperature, higher strain rate, and higher applied strain. This cannot be explained by the measured tortuosity of the recrystallization front. By contrast, higher stored energy after deformation can account for these observations, and others in past research. Hence, it is here proposed, for the first time, that higher dislocation density promotes annealing twinning through the higher density of microstructural discontinuities inside the deformed matrix. These should facilitate growth accidents. Lower SFE enhances twinning probability also in the annealing of hot-deformed austenite. The occurrence of twinning is not precluded even for the smallest recrystallized grain sizes (i.e., < 5 μm).
3. Among twin boundaries, Σ3 and Σ9 boundaries appear at the same rate during recrystallization. However, the density of Σ9 boundaries decays considerably faster during grain growth. This agrees with their higher interface energy and mobility, compared to Σ3 boundaries. In turn, this supports a driving role of twin boundary energy

and mobility in the elimination of twin boundaries upon grain growth.

4. Parent austenite reconstruction captures the CSL character of twin boundaries inside recrystallized grains, and its loss with plastic deformation. Furthermore, it produces the correct trends for both the density of twin boundaries, and their number per recrystallized grain. Tested trends include the evolution of twinning during recrystallization and subsequent grain growth, and the effect of applied strain.

CRediT authorship contribution statement

Pablo Garcia-Chao: Writing – review & editing, Writing – original draft, Visualization, Methodology, Investigation, Funding acquisition, Formal analysis, Data curation, Conceptualization. **Tuomo Nyyssönen:** Writing – review & editing, Visualization, Software, Methodology, Investigation, Formal analysis, Data curation. **Adam Ståhlkrantz:** Writing – review & editing, Methodology, Investigation, Data curation. **Hans Magnusson:** Writing – review & editing, Visualization, Validation, Supervision, Software, Methodology, Funding acquisition, Conceptualization.

Declaration of competing interest

On behalf of all authors, the corresponding author states that there is no conflict of interest.

Acknowledgements

Pablo Garcia-Chao acknowledges Jernkontoret (Swedish Iron and Steel Producers' Association) for funding his stay in Sweden, under the framework of the Överingenjören Gustaf Janssons Jernkontorsfond (March 2024). Part of this work was also funded by Swedish National Project "Full scale integrated modelling of metal working" (Finbeam2, Vinnova 2022-01600). The authors thank Johan Lönnqvist for help with the Gleeble work, and Dr. René de Kloe from EDAX/Gatan for help with the EBSD analysis. The authors are also grateful to Delft University of Technology and Tata Steel Nederland for the experimental work concerning the Ni-30Fe alloy.

Data availability

The raw/processed data required to reproduce these findings cannot be shared at this time as the data also forms part of an ongoing study.

References

[1] Y. Jin, B. Lin, M. Bernacki, G.S. Rohrer, A.D. Rollett, N. Bozzolo, Annealing twin development during recrystallization and grain growth in pure nickel, Mater. Sci. Eng. A 597 (2014) 295–303.
[2] A.D. Rollett, G.S. Rohrer, F.J. Humphreys, Recrystallization and Related Annealing Phenomena, 3rd ed., Elsevier Health Sciences, London, 2017.
[3] J.E. Burke, The formation of annealing twins, JOM 2 (1950) 1324–1328.
[4] H. Gleiter, The formation of annealing twins, Acta Metall. 17 (1969) 1421–1428.
[5] S. Mahajan, C.S. Pande, M.A. Imam, B.B. Rath, Formation of annealing twins in fcc crystals, Acta Mater. 45 (1997) 2633–2638.
[6] C.S. Pande, M.A. Imam, B.B. Rath, Study of annealing twins in FCC metals and alloys, Metall. Trans. A. 21 (1990) 2891–2896.
[7] Y. Jin, B. Lin, A.D. Rollett, G.S. Rohrer, M. Bernacki, N. Bozzolo, Thermomechanical factors influencing annealing twin development in nickel during recrystallization, J. Mater. Sci. 50 (2015) 5191–5203.
[8] V. Randle, Grain boundary engineering: an overview after 25 years, Mater. Sci. Technol. 26 (2010) 253–261.
[9] S. Mandal, A. Bhaduri, V. Subramanya Sarma, Role of twinning on dynamic recrystallization and microstructure during moderate to high strain rate hot deformation of a Ti-modified austenitic stainless steel, Metall. Mater. Trans. A 43 (2012) 2056–2068.
[10] D. Jia, W. Sun, D. Xu, L. Yu, X. Xin, W. Zhang, F. Qi, Abnormal dynamic recrystallization behavior of a nickel based superalloy during hot deformation, J. Alloys Compd. 787 (2019) 196–205.
[11] M. Schneider, J.-P. Couzinié, A. Shalabi, F. Ibrahimkhel, A. Ferrari, F. Körmann, G. Laplanche, Effect of stacking fault energy on the thickness and density of annealing twins in recrystallized FCC medium and high-entropy alloys, Scr. Mater. 240 (2024) 115844.
[12] N. Bozzolo, M. Bernacki, Viewpoint on the formation and evolution of annealing twins during thermomechanical processing of FCC metals and alloys, Metall. Mater. Trans. A 51 (2020) 2665–2684.
[13] I. Escobar-Moreno, E. Nieto-Valeiras, J. Llorca, Slip transfer and crack initiation at grain and twin boundaries during strain-controlled fatigue of solution-hardened Ni-based alloys, Acta Mater. 283 (2025) 120497.
[14] Y.J. Nie, F. Yang, L.X. Meng, Y.Z. Wang, L. Yin, Q.X. Shi, J.Y. Ma, W. Liang, L. W. Zheng, Hydrogen-enhanced densified deformation twins in 304L austenitic stainless steel fabricated by selective laser melting, Mater. Today Commun. 39 (2024) 109130.
[15] Q. Gao, Z. Liu, L. Sun, Q. Ma, H. Zhang, J. Bai, X. Lin, L. Yu, H. Li, Review on precipitates and high-temperature properties of alumina-forming austenitic stainless steel, J. Mater. Res. Technol. 25 (2023) 5372–5393.
[16] X. Li, Q. Ma, E. Liu, Z. Li, J. Bai, H. Li, Q. Gao, Order phase transition of HIP nickel-based powder superalloy during isothermal aging, J. Alloys Compd. 1010 (2025) 177269.
[17] Y. Jin, M. Bernacki, A. Agnoli, B. Lin, G.S. Rohrer, A.D. Rollett, N. Bozzolo, Evolution of the annealing twin density during δ-supersolvus grain growth in the nickel-based superalloy Inconel™ 718, Metals 6 (2015) 5.
[18] M.K. Rehman, H.S. Zurob, A novel approach to model static recrystallization of austenite during hot rolling of Nb microalloyed steel. Part I: Precipitate-free case, Metall. Mater. Trans. A 44 (2013) 1862–1871.
[19] C. Haase, M. Kühbach, L.A. Barrales-Mora, S.L. Wong, F. Roters, D.A. Molodov, G. Gottstein, Recrystallization behavior of a high-manganese steel: experiments and simulations, Acta Mater. 100 (2015) 155–168.
[20] H. Zurob, C. Hutchinson, Y. Brechet, G. Purdy, Modeling recrystallization of microalloyed austenite: effect of coupling recovery, precipitation and recrystallization, Acta Mater. 50 (2002) 3077–3094.
[21] A. Laasraoui, J. Jonas, Recrystallization of austenite after deformation at high temperatures and strain rates—analysis and modeling, Metall. Trans. A. 22 (1991) 151–160.
[22] G. Shankar, S. Sanandiya, L.A. Barrales-Mora, S. Suwas, Evolution of recrystallization texture in nickel-iron alloys: experiments and simulations, Philos. Mag. 103 (2023) 1787–1827.
[23] P. Garcia-Chao, J.J. Eipe, M. Krugla, C. Bos, J. Sietsma, W. Kranendonk, S. E. Offerman, Nucleation sites in the static recrystallization of a hot-deformed Ni-30 Pct Fe austenite model alloy, Metall. Mater. Trans. A 54 (2023) 2160–2177.
[24] M. Bhattacharyya, B. Langelier, G.R. Purdy, H.S. Zurob, Effect of Mn and C on grain growth in Mn steels, Metall. Mater. Trans. A 50 (2019) 905–914.
[25] M. Bhattacharyya, Y. Brechet, G.R. Purdy, H.S. Zurob, Austenite grain growth in high manganese steels, Metall. Mater. Trans. A 50 (2019) 5760–5766.
[26] H. Beladi, P. Cizek, A.S. Taylor, G.S. Rohrer, P.D. Hodgson, Static softening in a Ni-30Fe austenitic model alloy after hot deformation: microstructure and texture evolution, Metall. Mater. Trans. A 48 (2017) 855–867.
[27] D.L. Olmsted, E.A. Holm, S.M. Foiles, Survey of computed grain boundary properties in face-centered cubic metals—II: grain boundary mobility, Acta Mater. 57 (2009) 3704–3713.
[28] W. Charnock, J. Nutting, The effect of carbon and nickel upon the stacking-fault energy of iron, Metal Sci. J. 1 (1967) 123–127.
[29] M. Zohrevand, M. Aghaie-Khafri, F. Forouzan, E. Vuorinen, Microstructural evolutions under ultrasonic treatment in 304 and 316 austenitic stainless steels: impact of stacking fault energy, Steel Res. Int. 92 (2021) 2100041.
[30] G.M. de Bellefon, M.N. Gussev, A.D. Stoica, J.C. van Duysen, K. Sridharan, Examining the influence of stacking fault width on deformation twinning in an austenitic stainless steel, Scr. Mater. 157 (2018) 162–166.
[31] A.E. Pontini, J.D. Hermida, X-ray diffraction measurement of the stacking fault energy reduction induced by hydrogen in an AISI 304 steel, Scr. Mater. 37 (1997) 1831–1837.
[32] N. Bozzolo, N. Souaï, R.E. Logé, Evolution of microstructure and twin density during thermomechanical processing in a γ-γ'nickel-based superalloy, Acta Mater. 60 (2012) 5056–5066.
[33] Z. Li, L. Zhang, N. Sun, Y. Sun, A. Shan, Effects of prior deformation and annealing process on microstructure and annealing twin density in a nickel based alloy, Mater. Charact. 95 (2014) 299–306.
[34] M. Kubota, K. Ushioda, G. Miyamoto, T. Furuhara, Analysis of recrystallization behavior of hot-deformed austenite reconstructed from electron backscattering diffraction orientation maps of lath martensite, Scr. Mater. 112 (2016) 92–95.
[35] F. Niessen, T. Nyyssönen, A.A. Gazder, R. Hielscher, Parent grain reconstruction from partially or fully transformed microstructures in MTEX, J. Appl. Crystallogr. 55 (2022) 180–194.
[36] R. Hielscher, T. Nyyssönen, F. Niessen, A.A. Gazder, The variant graph approach to improved parent grain reconstruction, Materialia 22 (2022) 101399.
[37] R.M. Birch, T.B. Britton, W.J. Poole, Improving parent-austenite twinned grain reconstruction using electron backscatter diffraction in low carbon austenite, Scr. Mater. 257 (2025) 116459.
[38] D. Sun, Z. Zhou, K. Zhang, X. Yang, X. Liu, Z. Guo, J. Gu, Novel reconstruction approaches of austenitic annealing twin boundaries and grain boundaries of ultrafine grained prior austenite, Mater. Des. 227 (2023) 111692.
[39] M. Taylor, A.D. Smith, J.M. Donoghue, T.L. Burnett, E.J. Pickering, In-situ heating-stage EBSD validation of algorithms for prior-austenite grain reconstruction in steel, Scr. Mater. 242 (2024) 115924.
[40] A.S. Taylor, P. Cizek, P.D. Hodgson, Comparison of 304 stainless steel and Ni–30 wt.% Fe as potential model alloys to study the behaviour of austenite during thermomechanical processing, Acta Mater. 59 (2011) 5832–5844.

[41] P. Mannan, G. Casillas, E.V. Pereloma, The effect of Nb solute and NbC precipitates on dynamic and metadynamic recrystallisation in Ni-30Fe-Nb-C model alloys, Mater. Sci. Eng. A 700 (2017) 116–131.
[42] E.V. Pereloma, P. Mannan, G. Casillas, A.A. Saleh, Particle stimulated nucleation during dynamic and metadynamic recrystallisation of Ni-30% Fe-Nb-C alloy, Mater. Charact. 125 (2017) 94–98.
[43] H. Beladi, P. Cizek, P.D. Hodgson, New insight into the mechanism of metadynamic softening in austenite, Acta Mater. 59 (2011) 1482–1492.
[44] W. Chen, B. Hu, C. Jia, C. Zheng, D. Li, Continuous dynamic recrystallization during the transient deformation in a Ni-30% Fe austenitic model alloy, Mater. Sci. Eng. A 751 (2019) 10–14.
[45] M. Yonemura, S. Sugano, I. Yamaguchi, H. Toyokawa, H. Saito, High-energy X-ray dynamics of the recovery and recrystallization behaviors of steels subjected to uniaxial hot compression and isothermal annealing, Metall. Mater. Trans. A (2025) 1–12.
[46] I. Yamaguchi, M. Yonemura, Recovery and recrystallization behaviors of Ni–30 mass pct Fe alloy during uniaxial cold and hot compression, Metall. Mater. Trans. A 52 (2021) 3517–3529.
[47] A. Godfrey, Edge preservation near triple junctions during orientation averaging of EBSP data, Scr. Mater. 50 (2004) 1097–1101.
[48] D.G. Brandon, The structure of high-angle grain boundaries, Acta Metall. 14 (1966) 1479–1484.
[49] D.P. Field, P.B. Trivedi, S.I. Wright, M. Kumar, Analysis of local orientation gradients in deformed single crystals, Ultramicroscopy 103 (2005) 33–39.
[50] R.J. Wakelin, E.L. Yates, A study of the order-disorder transformation in Iron-Nickel alloys in the region FeNi3, Proc. Phys. Soc. Sect. B 66 (1953) 221.
[51] D. Nettleton, Chapter 6 - Selection of Variables and Factor Derivation, Commercial Data Mining: Processing, Analysis and Modeling for Predictive Analytics Projects, Elsevier Inc., 2014.
[52] S. Sarkar, M. Militzer, Microstructure evolution model for hot strip rolling of Nb–Mo microalloyed complex phase steel, Mater. Sci. Technol. 25 (2009) 1134–1146.
[53] S. Sarkar, A. Moreau, M. Militzer, W. Poole, Evolution of austenite recrystallization and grain growth using laser ultrasonics, Metall. Mater. Trans. A 39 (2008) 897–907.
[54] V. Shah, K. Sedighiani, J.S. Van Dokkum, C. Bos, F. Roters, M. Diehl, Coupling crystal plasticity and cellular automaton models to study meta-dynamic recrystallization during hot rolling at high strain rates, Mater. Sci. Eng. A 849 (2022) 143471.
[55] W.-F. Shen, C. Zhang, L.-W. Zhang, Y.-N. Xia, Y.-F. Xu, X.-H. Shi, Metadynamic recrystallization of Nb–V microalloyed steel during hot deformation, J. Mater. Res. 32 (2017) 656–665.
[56] A. Smith, S.E. Kruger, J. Sietsma, S. van Der Zwaag, Laser-ultrasonic monitoring of austenite recrystallization in C–Mn steel, ISIJ Int. 46 (2006) 1223–1232.
[57] Q. Bai, Q. Zhao, S. Xia, B. Wang, B. Zhou, C. Su, Evolution of grain boundary character distributions in alloy 825 tubes during high temperature annealing: is grain boundary engineering achieved through recrystallization or grain growth? Mater. Charact. 123 (2017) 178–188.
[58] Q. Li, J. Cahoon, N. Richards, Effects of thermo-mechanical processing parameters on the special boundary configurations of commercially pure nickel, Mater. Sci. Eng. A 527 (2009) 263–271.
[59] R.L. Fullman, J.C. Fisher, Formation of annealing twins during grain growth, J. Appl. Phys. 22 (1951) 1350–1355.
[60] T. Nyyssönen, M. Malmström, D. Lindell, A. Jansson, J. Lönnqvist, L. Bäcke, B. Hutchinson, Significance of annealing twins in laser ultrasonic measurements of grain size in high-strength low-alloy steels, Appl. Sci. 13 (2023) 3901.
[61] Y. Jin, M. Bernacki, G.S. Rohrer, A.D. Rollett, B. Lin, N. Bozzolo, Formation of Annealing Twins during Recrystallization and Grain Growth in 304L Austenitic Stainless Steel, Materials Science Forum, Trans Tech Publ, 2013, pp. 113–116.
[62] H. Pan, Y. He, X. Zhang, Interactions between dislocations and boundaries during deformation, Materials 14 (2021) 1012.
[63] Y.-C. Xia, X.-M. Chen, Y.-C. Lin, X.-Z. Lu, Evolution of annealing twins in a hot deformed nickel-based superalloy, Materials 15 (2021) 7.
[64] B. Schulz, N. Haghdadi, T. Leitner, M. Hafok, S. Primig, Dynamic recrystallisation via nucleation at distorted twins in a Ni-based superalloy, J. Alloys Compd. 936 (2023) 168318.
[65] B. Lin, Y. Jin, C.M. Hefferan, S.F. Li, J. Lind, R.M. Suter, M. Bernacki, N. Bozzolo, A. D. Rollett, G.S. Rohrer, Observation of annealing twin nucleation at triple lines in nickel during grain growth, Acta Mater. 99 (2015) 63–68.
[66] D.L. Olmsted, S.M. Foiles, E.A. Holm, Survey of computed grain boundary properties in face-centered cubic metals: I. Grain boundary energy, Acta Mater. 57 (2009) 3694–3703.
[67] G.S. Rohrer, E.A. Holm, A.D. Rollett, S.M. Foiles, J. Li, D.L. Olmsted, Comparing calculated and measured grain boundary energies in nickel, Acta Mater. 58 (2010) 5063–5069.
[68] P. Garcia-Chao, The Formability of Magnesium and Magnesium-Rare Earth Alloys under the Strain Path of Cold Rolling, the University of Manchester (United Kingdom), 2018.
[69] B. Wang, H. Liu, Y. Zhang, B. Zhou, L. Deng, C. Wang, J. Chen, Y. Zhang, Effect of grain size on twinning behavior of pure titanium at room temperature, Mater. Sci. Eng. A 827 (2021) 142060.
[70] D.-W. Suh, T. Inoue, S. Torizuka, A. Ohmori, K. Nagai, Serration of grain boundary in Ni-30Fe alloy through high temperature deformation, ISIJ Int. 42 (2002) 1026–1032.
[71] A. Hamed, S. Rayaprolu, G. Winther, A. El-Azab, Impact of the plastic deformation microstructure in metals on the kinetics of recrystallization: a phase-field study, Acta Mater. 240 (2022) 118332.
[72] J. Lee, S.I. Hong, H.S. Kim, Bulging of grain boundaries and core-shell dislocation structures enhance mechanical properties of equiatomic high-entropy alloys, Int. J. Plast. 185 (2025) 104224.
[73] D.-W. Suh, S. Torizuka, A. Ohmori, T. Inoue, K. Nagai, Dynamic restoration process of Ni-30Fe alloy during hot deformation, ISIJ Int. 42 (2002) 432–439.
[74] M.A. Charpagne, A.T. Polonsky, M.P. Echlin, S. Jacomet, J. De Jaeger, M. De Graef, N. Bozzolo, T.M. Pollock, Growth accidents induced by primary γ' precipitates in a polycrystalline nickel-based superalloy, Scr. Mater. 186 (2020) 109–113.